Deltares

Influence of water depth on the wave height, wave run-up and front velocities

Influence of water depth on the wave height, wave run-up and front velocities

Author(s)
Madelief Doeleman
Joost den Bieman

Influence of water depth on the wave height, wave run-up and front velocities

Client	Rijkswaterstaat Water, Verkeer en Leefomgeving
Contact	De heer M. Bottema
Reference	KPP-Versterking Onderzoek Waterveiligheid, deelproject ‘Invloed waterdiepte op golfoverslag’
Keywords	Waves, wave height, wave run-up height, front velocities, influence of water depth, shallow water, COM

Document control	
Version	1.0
Date	14-09-2022
Project nr.	11208034-011
Document ID	11208034-011-ZWS-0001
Pages	52
Classification	
Status	final

Author(s)		
	M.W. Doeleman	
	J.P. den Bieman	

Samenvatting

In Nederland zijn honderden kilometers dijk bekleed met een grasbekleding waaruit sterkte wordt ontleend in het geval van golfbelasting. Het is van belang om de kans op falen van de grasbekleding onder golfbelasting zo goed mogelijk in te kunnen schatten aangezien dit veelal een aanzienlijke faalkansreductie oplevert in de keten van gebeurtenissen die tot een grootschalige overstroming kunnen leiden. Indien deze kans niet goed wordt ingeschat kan dit leiden tot óf een (onbewuste) situatie waarbij de daadwerkelijke faalkans groter is dan de volgens de wettelijke normen gehanteerde faalkans óf tot een inefficiënt dijkontwerp, ofwel onnodige versterking van een dijk.

Voor het bepalen van de faalkans van een dijk is uitgebreid onderzoek gedaan naar de typische golfoploophoogte $R_{2\%}$ en met name het (gemiddelde) overslagdebiet. De resultaten van deze onderzoeken zijn samengevoegd in de EurOtop handleiding (EurOtop, 2018) en de TAW (2002). Om het falen van de grasbekleding nauwkeuriger in te schatten, wordt een overstap gemaakt naar het gebruik van de Cumulatieve Overbelasting Methode (COM). In de COM wordt elke golfoploop (GEBU) of overslaande golf (GEKB) tijdens een periode van golfbelasting op de dijk beschouwd. De bijdrage aan de totale schade van elk gebeurtenis is afhankelijk van de frontsnelheid behorend bij de betreffende gebeurtenis. Voor het toepassen van de COM is het dus belangrijk om zo nauwkeurig mogelijk de snelheden te voorspellen van de golven die de dijk oplopen op het buitentalud en die (soms) de kruin overslaan en langs het binnentalud naar beneden lopen. Voorgaand onderzoek, dat is samengevat in de EurOtop handleiding en TAW (2002) dient dus, voor zover mogelijk, vertaald te worden naar de context van de COM.

In dit rapport is de invloed van ondiepe voorlanden op de golfhoogte, golfoploophoogte en snelheden binnen de context van de COM onderzocht. Dit onderzoek is onderdeel van het KPP (Kennis Primaire Processen) VOW (Versterking Onderzoek Waterveiligheid). Binnen het KPP-VOW project is tussen 2017-2019 de invloed van ondiepe voorlanden op het overslagdebiet onderzocht. Dit is samengevat door Van Steeg *et al.* (2020). In het voorliggende rapport zijn drie datasets, die bestaan uit klein- en grootschalige fysieke experimenten en gevalideerde numerieke simulaties, geanalyseerd. De beschouwde datasets bestrijken een grote range voor verschillende dimensieloze parameters, waaronder de meest belangrijke het Iribarren getal, golfsteilheid, relatieve waterdiepte en relatieve kruinhoogte. De modelopstellingen van de geanalyseerde datasets zijn opgezet met vlakke bodems, een glad talud en zijn belast met langkammige golven. Om de invloed van ruwheid, bermen, variaties in de dwarsdoorsnede en schuine golfinval te onderzoeken worden aanvullende (fysieke en numerieke) experimenten aanbevolen.

Dit onderzoek concludeert dat de gemeten golfhoogteverdelingen redelijk in overeenstemming zijn met bestaande literatuur. In diep water is de **golfhoogteverdeling** grofweg Rayleigh verdeeld. In ondiep water is de golfhoogteverdeling redelijk in overeenstemming met de ondiep water golfhoogteverdelingen van Battjes en Groenendijk (2000) en Karmpadakis *et al.* (2022). De datasets die in dit onderzoek worden beschouwd vallen echter niet binnen het geldigheidsbereik van beide verdelingen. Het wordt aanbevolen om de validiteit van de (te gebruiken) theoretische golfhoogteverdeling kritisch te beoordelen. Indien voor niet gevalideerde situaties een theoretische verdeling wordt gebruikt, is een verschil tussen de theoretische voorspelling en praktijk mogelijk. Hiernaast is het effect van (lange) horizontale bodems op de golfhoogteverdeling onbekend. Het wordt daarom aanbevolen om de ontwikkeling van de golfhoogteverdeling over horizontale bodems experimenteel te onderzoeken. Dit onderzoek is bijvoorbeeld relevant in de Waddenzee.

Voor kleiner wordende waterdieptes laat de beschouwde data zien dat (i) de **golfoploophoogteverdeling** de afwijking van de golfhoogteverdeling ten opzichte van Rayleigh niet volledig lijkt te volgen. In diep water is de golfoploophoogteverdeling min of meer Rayleigh verdeeld. In ondiep water vlakt het rechter deel van de verdeling af. Hiernaast laat dit onderzoek zien dat (ii) in opdiep water de golfoploophoogteverdeling significant minder afwijkt van Rayleigh (gebaseerd op $R_{u2\%}$) dan de golfhoogteverdeling (gebaseerd op Rayleigh volgens Longuet-Higgins (1952)). Ook wordt aangetoond dat (iii) er door een gebrek aan golfoploop data in de lage overschrijdingskansen er niet met vertrouwen een nieuwe relatie tussen de golfhoogte- en golfoploophoogteverdeling kan worden afgeleid op basis van de data beschouwd in dit rapport. Dit komt doordat twee van de drie beschouwde datasets zijn gegenereerd in de context van onderzoek naar het golfoverslagdebiet. De testen in deze datasets missen dus een groot deel van de golfoploophoogte informatie. Het wordt daarom aanbevolen om aanvullende datasets met 'oneindig' hoge kruinhoogtes te genereren om een relatie te kunnen afleiden tussen de golfhoogte, golfoploophoogte en frontsnelheid.

De conclusie voor de **frontsnelheidsverdeling** is drieledig. (i) De frontsnelheidsverdeling voor diep en ondiep water is niet volledig Rayleigh (gebaseerd op $U_{2\%}$) verdeeld. (ii) De vorm van de frontsnelheidsverdeling is onafhankelijk van de relatieve waterdiepte. (iii) De relatie tussen de frontsnelheids- en de golfoploophoogteverdeling is sterker en de testen laten weinig spreiding zien, dan de relatie tussen de frontsnelheids- en de golfhoogteverdeling.

De invloed van de relatieve waterdiepte werkt dus sterk door in de vorm van de golfhoogteverdeling, in mindere mate in de vorm van de golfoploophoogteverdeling en niet in de vorm van de frontsnelheidsverdeling. Omdat eerder onderzoek (van Steeg et al, 2020) aangaf dat de waterdiepte wel degelijk significante invloed heeft op oploop en overslag wordt aanbevolen om alternatieve normalisatie methoden te onderzoeken om, naast de vorm van de verdelingen, ook de invloed van waterdiepte vast te stellen op de schaling van de golfoploophoogte- en frontsnelheidsverdeling.

Tenslotte concludeert dit onderzoek op basis van de beschikbare data dat de *relaties* tussen de golfhoogte- en golfoploophoogteverdeling, en de golfoploophoogte- en frontsnelheidsverdeling niet significant beïnvloed worden door de relatieve waterdiepte (H_{m0}/d), anders dan de gereduceerde significante golfhoogte door golfbreking. Daarom kan er niet simpelweg worden aangenomen dat de golfoploophoogte en frontsnelheidsverdelingen kunnen worden beschreven op basis van de theoretische ondiep water verdeling voor golfhoogte.

Summary

The Netherlands contains hundreds of kilometers of dikes with a grass cover. This grass cover protects the dike against the loads caused by (overtopping) waves. Hence, it is important to be able to accurately estimate the probability of failure of the grass cover, since this concerns the initial mechanism in the failure pathway where dike erosion eventually leads to a large flooding of the hinterland. Inaccurate failure probabilities of the grass cover can lead either to dikes that do not adhere to the legally required maximum probability of flooding or to uneconomical dike designs.

To determine the failure probability on a dike, extensive research has been performed on the typical wave run-up height $R_{2\%}$ and predominantly the (mean) overtopping rate q. The results are merged into the EurOtop Manual (EurOtop, 2018) and TAW (2002). To more accurately estimate the failure probability of the grass cover, the Cumulative Overload Method (COM / Cumulatieve Overbelasting Methode) will be used. In the COM, each wave run-up (GEBU) or overtopping (GEKB) event within the considered loading period of the dike is considered. The contribution to the total damage of each event is dependent on the flow velocity belonging to that event. Thus, when applying the COM it is important to be able to accurately predict the velocities of waves that run up the outer dike slope and (sometimes) overtop the dike crest and subsequently run down the inner dike slope. Previous research that is summarised in the EurOtop Manual and TAW (2002) should thus be translated to the context of the COM where possible.

This report researches the influence of shallow foreshores on the wave height, wave run-up height and velocities in the context of the COM. This research is part of the KPP (Kennis Primaire Processen / knowledge primary processes) VOW (Versterking Onderzoek Waterveiligheid / strengthening flood safety research) project. Within the KPP-VOW project, the influence of shallow foreshores on the overtopping discharge was researched between 2017-2019. This is summarised by Van Steeg *et al.* (2020). Three datasets consisting of small- and large-scale physical model experiments and validated numerical simulations were analyzed. The datasets cover a wide range of dimensionless parameters, most important among them the Iribarren number, wave steepness, relative water depth and relative crest height. The tested 1D models include flat beds, smooth slopes and are forced with long-crested waves. To research the influence of roughness, berms, cross-shore variations and oblique wave attack on the influence of water depth additional (physical and numerical) experiments are recommended.

This research concludes that the measured wave heights are in accordance with theory. In deep water the **wave height distribution** is roughly Rayleigh distributed. In shallow water the wave height distribution is in reasonable accordance with the shallow water distributions of Battjes and Groenendijk (2000) and Karmpadakis *et al.* (2022). The datasets considered in this research are however not within the validity range of both distributions. It is recommended to critically assess the validity of the (to be) used theoretical shallow water distribution. If a theoretical distribution is used for unvalidated situations differences between theory and practice is expected Also, the effect of a (long) horizontal bed on the wave height distribution is yet unknown. It is therefore recommended to experimentally research the development of the wave height distribution over long flat beds. This is relevant in areas such as the Wadden Sea.

For smaller water depths, the analyzed data shows that (i) the **wave *run-up* height distribution** seems to not entirely follow the deviation of the wave height distribution w.r.t. a

Rayleigh distribution. In deep water the wave run-up height exceedance distribution is a relative straight line on a Rayleigh x-axis. In shallow water, the right tail of the wave run-up height distribution flattens. In addition, it is found that (ii) the wave run-up height distribution deviates significantly less from Rayleigh (based on $R_{u2\%}$) for shallow water conditions than the wave height distribution (based on Rayleigh following Longuet-Higgins (1952)). Also, it is shown that (iii) a new relation between the wave height and wave *run-up* height distribution cannot be derived with confidence due to a lack of run-up data with low exceedance probabilities. This is because two out of three datasets considered have been generated in the context of wave overtopping research. These tests therefore lack a significant part of the wave run-up height information. It is therefore recommended to generate additional datasets with 'infinitely' high crests to properly derive a relation between the wave height, wave run-up height and front velocity.

The conclusion for the **front velocity distribution** in shallowing water is threefold. (i) The front velocity distribution for deep and shallow water is not entirely Rayleigh distributed (based on $U_{2\%}$). (ii) The shape of the front velocity distribution does not depend on the relative water depth. (iii) The relation between the front velocity and wave *run-up* height distribution is stronger and the experimental data shows less scatter, than the relation between the front velocity and the wave height distribution.

The relative water depth therefore strongly influences the shape of the wave height distribution, to a lesser extent the shape of the wave run-up height distribution and does not influence the shape of the front velocity distribution. Since previous research (van Steeg et al, 2020) pointed at a significant influence of water depth on wave runup and overtopping, it is recommended to investigate alternative normalization methods to be able to assess the influence of water depth on the scaling of the wave run-up height and velocity distributions, besides the shape aspects that were already investigated in this report.

Lastly, this research concludes, based on the available data, that the *relations* between the wave height and wave *run-up* height distribution, and wave *run-up* height and front velocity distribution seem to not be significantly influenced by the relative water depth (H_{m0}/d), besides the reduced significant wave height due to wave breaking. Therefore, it cannot simply be assumed that the wave run-up height and front velocity distributions follow the theoretical shallow water wave height distribution.

Contents

1 Introduction

1.1 Overview of current projects concerning wave run-up and flow velocities

The Netherlands contains hundreds of kilometers of dikes with a grass cover. This grass cover protects the dike against the loads caused by (overtopping) waves. Hence, it is important to be able to accurately estimate the probability of failure of the grass cover, since this concerns the initial mechanism in the failure pathway where dike erosion eventually leads to a large flooding of the hinterland. Inaccurate failure probabilities of the grass cover can lead to either dikes that do not adhere to the legally required maximum probability of flooding or uneconomical dike designs.

Within BOI – the toolbox for safety assessment and design of flood defenses in The Netherlands – the failure of grass cover is considered separately for the outer dike slope on the one hand, and the dike crest and inner slope on the other hand. These initial failure mechanisms are named GEBU (Gras Erosie BUitentalud / grass erosion outer slope) and GEKB (Gras Erosie Kruin en Binnentalud / grass erosion crest and inner slope), as indicated in Figure 1.1. Note that GEBU covers grass erosion due to both wave impacts and wave run-up. Only the latter is within the scope of these projects, so when GEBU is mentioned, only the grass erosion due to wave run-up is meant.

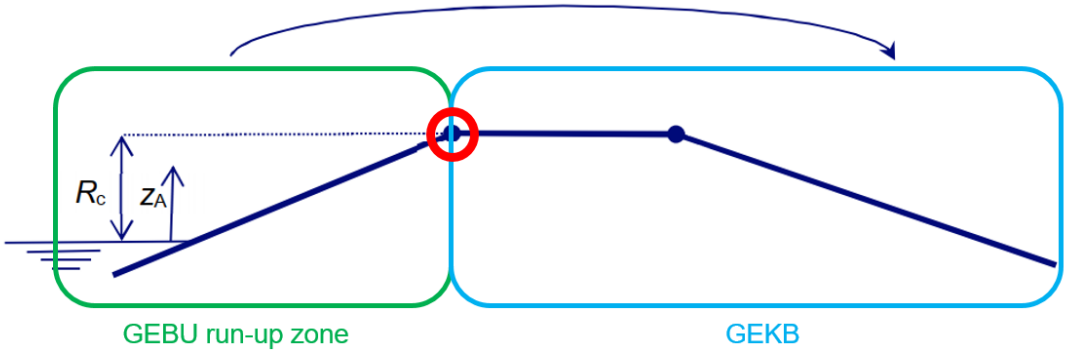

Figure 1.1 Schematic depiction of a dike and the domains of the GEBU run-up zone and GEKB initial failure mechanisms. The discontinuity in the existing velocity descriptions occurs on the outer crest line (red circle).

Both of these failure mechanisms will use the Cumulative Overload Method (COM / Cumulatieve Overbelasting Methode) to calculate the failure of the grass revetment. In the COM, each wave run-up (GEBU) or overtopping (GEKB) event within the considered loading period of the dike is considered. The contribution to the total damage of each event is dependent on the flow velocity belonging to that event. Thus, when applying the COM it is important to be able to accurately predict the velocities of waves that run up the outer dike slope and (sometimes) overtop the dike crest and subsequently run down the inner dike slope.

Currently, GEBU and GEKB apply two different expressions to predict the flow velocity. These two expressions result in a discontinuity in the predicted flow velocity on the outer crest line of the dike. This is both physically unrealistic and impractical, and as such is mentioned as an issue in the ‘Rode draad overstroming door dijkerosie’ (Deltares, RWS-WVL & HWBP, 2022). Hence, research was started (Deltares, 2021a; Deltares, 2021b) to come to a harmonized expression for velocities that can be used both in GEBU and in GEKB. This effort and research related to it is continued and is divided over three different projects in 2022. Deriving a new harmonized velocity expression is being done as a part of the KvK (Kennis voor Keringen /

knowledge for flood defenses) project. Within the KPP (Kennis Primaire Processen / knowledge primary processes) VOW (Versterking Onderzoek Waterveiligheid / strengthening flood safety research) project two subprojects on this subject are present. One is dedicated to identifying the influence of shallow water on run-up heights and velocities, the other to a study of the background of the different influence and acceleration factors (in)directly used within the COM method for GEBU and GEKB. These projects exchange knowledge extensively, to maintain cohesion on this subject. It is foreseen that the knowledge developed within these projects, when mature enough, will be adopted and implemented by the BOI project in the near future. The (expected) deliverables of these projects are listed below.

- KvK 'stroomsnelheden grasbekleding' (11208057-037)
  - Report technical background harmonized velocity formula (Deltares, 2022a)
  - Report consequences of switch to harmonized expression (Deltares, 2022b)
- KPP-VOW 'parameters stroomsnelheden dijktalud' (11208034-001)
  - Report technical background influence and acceleration factors (Deltares, 2022c)
- KPP-VOW 'invloed waterdiepte op golfoverslag' (11208034-011)
  - Report data analysis of shallow water data for wave run-up (this report)

1.2 Scope of this research

To determine the failure probability on a dike, extensive research has been performed on the typical wave run-up height $R_{2\%}$ and (mean) overtopping rate q. The studies include tens of thousands of tests in wave flumes and basins to determine relations between the hydraulic loads, dike geometry, roughness on the one hand and the wave run-up height and overtopping discharge on the other hand. These studies are merged into the Eurotop Manual (Eurotop, 2018) and TAW (2002). The influence of shallow foreshores is investigated between 2017-2019 and summarised by Van Steeg *et al.* (2020). It is concluded that the water depth at the toe of the dike significantly influences the overtopping discharge.

To more accurately estimate the failure probability of the grass cover, the Cumulative Overload Method (COM / Cumulatieve Overbelasting Methode) is introduced. As stated in Section 1.1, in the COM, each wave run-up (GEBU) or overtopping (GEKB) event within the considered loading period of the dike is considered. The contribution to the total damage of each event is dependent on the flow velocity belonging to that event. Thus, when applying the COM it is important to be able to accurately predict the velocities of waves that run up the outer dike slope and (sometimes) overtop the dike crest and subsequently run down the inner dike slope.

Within this report, the influence of shallow foreshores on the wave height, wave run-up height and velocities in the context of the COM is researched. It is noted that wave impact is not considered. The research question and sub research questions are defined as follows:

- Can the influence of water depth on the wave run-up height and front velocity be accounted for in the COM?
  - What is the influence of water depth on the wave height and wave run-up height distribution?
  - How does this influence affect the front velocity distribution?

To answer these research questions three datasets with varying water depths are analysed. The datasets are described in Chapter 2. Following, all 47 tests are processed to obtain the wave height, wave run-up and front velocity distribution. The processing methods are summarised in Chapter 3. In Chapter 4 a relation between the wave height and wave run-up height distribution is determined. In Chapter 5 the influence of water depth for the wave run-up height and front velocity distribution is investigated. Additionally, recent research on infra-

gravity waves are elaborated upon in Chapter 6. Chapter 7 concludes with recommendations, a discussion and conclusions.

2 Datasets including varying water depths studied in this research

This chapter describes and assesses all available (and known) datasets that can be processed to wave run-up timeseries and that include variations in relative water depths. The datasets consist of small- and large-scale physical model experiments and validated numerical simulations using a CFD (Computational Fluid Dynamics) model OpenFOAM with the Wave2Foam toolbox (Jacobsen, 2012). The wave heights are measured using (numerical) wave gauges. The wave run-up and corresponding velocities are measured using a video camera for the physical model experiments and with a numerical step gauge for the numerical dataset.

The datasets cover a wide range in dimensionless parameters, most important among them the Iribarren number ($\xi_{m-1.0} = \tan(\alpha)/\sqrt{s_{m-1.0}}$), wave steepness ($s_{m-1.0}$), relative water depth (d/H_{m0}) and relative crest height (R_c/H_{m0}) based on the hydraulic conditions measured at the toe and dike outer slope angle α. Figure 2.1 shows the ranges of all the datasets used in the overarching front velocity derivation (Deltares, 2022a). Each dot represents one test. The 47 black dots in the figure show the dimensionless parameters of the datasets used in this research. It is noted that the figure is cut-off at 5.5. Experiments or numerical simulations with a higher (infinite) relative water depth and crest height are not shown. This is the case for (a number of) Delta Flume 2022 tests.

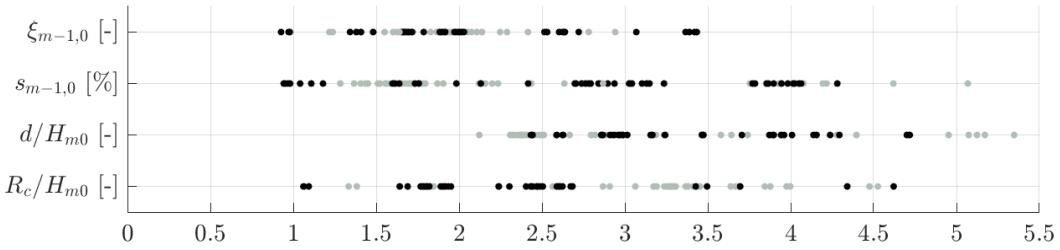

Figure 2.1 Dimensionless parameter range of available datasets including varying water depth (black dots) used in this research. The grey dots represent the tests of additional datasets used in the overarching Deltares (2022a) research. The parameters are measured at the toe of the dike.

To investigate the presence of bias for breaking and non-breaking waves, the breaker parameter versus the relative water depth is plotted in Figure 2.2. For a breaker parameter, $\xi_{m-1,0} < 1.73$, incoming wave fields are of breaking nature (and $\xi_{m-1,0} > 1.73$ not). Note that the transition point of $\xi_{m-1,0} = 1.73$ only holds for datasets with normal incident waves on a dike with a smooth slope and without a berm, which is the case of the datasets considered. Figure 2.2 shows that for $H_{m0}/d > 0.2$, a large range in breaker parameter ($0.2 < \xi_{m-1,0} < 3.4$) with some gaps in between is covered. For deep water, only tests with a limited range are available.

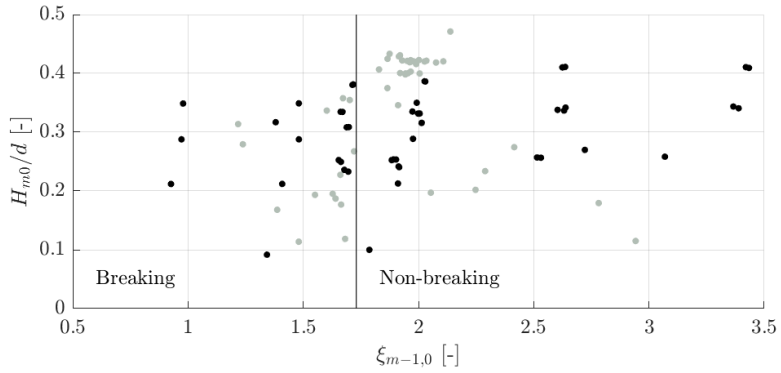

Figure 2.2 Overview of the breaker parameter versus the relative water depth. The black dots represent the tests of the available datasets used in this research. The grey dots show all tests used in the overarching Deltares (2022a) research. The parameters are measured at the toe of the dike.

2.1 Data Set 1: Scheldt Flume 2018

To assess the influence of water depth on the overtopping discharge, small-scale physical experiments are performed in the Scheldt Flume at Deltares (Deltares, 2018; Van Steeg et al. 2020). As the focus of the tests is on the overtopping discharge, the relative crest height is limited to ensure waves to overtop the dike. However, this means that the (maximum) run-up height is not measured during these overtopping events. The physical model consists of a smooth impermeable dike with a slope of 1:3. In front of the dike a foreshore is constructed that consists of a sloping step followed by a long horizonal bottom. The model setup can be found in Appendix A. In addition to overtopping measurements, a video camera recorded the wave run-up area.

Table 2.1: Overview physical dataset Scheldt Flume 2018

IWD Scheldt Flume 2018	
Total tests	31
Foreshore	Sloping 1:10 step followed by a horizontal bottom
Slope and material	1:3, smooth slope
Freeboard (R_c/H_{m0})	1.8 - 2.7
Water depth (H_{m0}/d)	0.23 – 0.41
Breaker parameter ($\xi_{m-1,0}$)	1.7 – 3.4
Steepness ($s_{m-1,0}$)	1% - 4%
Wave forcing	JONSWAP spectrum
Measurement technique	Video / AI Technique
Test program	2x R_c, 3x water depth, 4x steepness for H_{m0}/d = 0.4, 6x steepness for H_{m0}/d < 0.4.

2.2 Data Set 2: Scheldt Flume OpenFOAM 2019

To add to Data Set 1, numerical simulations are performed to obtain a larger range in terms of geometry (see slope in the table below) and typical dimensionless parameters (Deltares, 2019). The numerical data is simulated using OpenFOAM and validated using the physical experiments as described in Section 2.1. It is noted that the overall numerical research also included a variation in crest height, and therefore nine more tests than analysed in this research. As the nine additional tests with a smaller relative crest height contain much more

overtopping (less measurable run-up events), these simulations are not considered in this report. The data set contains the water depth at several locations along the slope and therefore also the wave run-up. The model setup can be found in Appendix A.

Table 2.2: Overview numerical dataset Scheldt Flume 2019

IWD OpenFOAM Scheldt Flume 2019	
Total tests	9
Foreshore	Sloping 1:10 step followed by a horizontal bottom
Slope and material	1:3 1:4 & 1:6, smooth slope
Freeboard (R_c/H_{m0})	1.1 – 2.3
Water depth (H_{m0}/d)	0.21 - 0.35
Breaker parameter ($\xi_{m-1,0}$)	0.9 – 2.0
Steepness ($s_{m-1,0}$)	2.8% - 3.2%
Wave forcing	JONSWAP spectrum
Measurement technique	Numerical wave gauges
Test program	3x water depth, 3x slope

2.3 Data Set 3: Delta Flume 2022

To add to the available datasets that contain run-up timeseries and varying water depths, additional large-scale physical experiments are performed in the spring of 2022. Furthermore, these tests are performed to assess potential scale-effects between the small-scale Scheldt Flume and large-scale Delta Flume. The test program and model set-up are shown in Appendix A. The wave run-up is captured by a video camera and for some of the tests with a step gauge. In this research only the video data is used to determine the run-up and velocities.

Table 2.3: Overview physical dataset Delta Flume 2022

IWD Delta Flume 2022	
Total tests	7
Foreshore	Horizontal bottom
Slope and material	1:3.6, smooth sand cement
Freeboard (R_c/H_{m0})	∞ (no overtopping waves)
Water depth (H_{m0}/d)	0.09 – 0.34
Breaker parameter ($\xi_{m-1,0}$)	1.3 - 2.7
Steepness ($s_{m-1,0}$)	1% - 4.3%
Wave forcing	JONSWAP spectrum
Measurement technique	Video / AI technique
Test program	3x water depth, 3x steepness for $H_{m0}/d = 0.33$, 2x steepness for $H_{m0}/d < 0.33$

3 Data analysis - method

This chapter elaborates on the analysis methods that are used in this research. First it is discussed how the wave height exceedance distribution at the dike toe is obtained. Following that, the derivation of run-up and front velocities is shown. Lastly, scale effects for the wave height, wave run-up height and front velocities between small- and large-scale physical modelling facilities are discussed.

3.1 Deriving the wave height exceedance distribution

For all datasets, the wave height near the dike toe is measured using a set of four wave gauges. As the surface elevation signal of one wave gauge contains incoming and reflected waves (due to the wave reflection at the dike structure), the total signal is separated using the set of four gauges according to the ELA method (Eldrup & Lykke Andersen, 2018; De Ridder et al., 2022). Individual wave heights now follow from a (preferred) zero-down crossing analysis (Holthuijsen, 2007). Sorting the wave heights and using the total number of waves in the signal, the exceedance distribution is derived. Spectral parameters, such as the spectral wave period, $T_{m-1,0}$, and the significant wave height, H_{m0}, are calculated by a Fourier analysis on the identified incoming surface elevation signal.

It is noted that the set of wave gauges is not directly located at the toe of the modelled dike and are spaced over a certain distance of approximately 0.5 times the wave length. Also, shallow water wave height distributions (composite/curved on Rayleigh axis) are expected to redistribute over horizontal bottoms to the deep water Rayleigh distribution (straight line on Rayleigh axis), given enough propagation distance. This is in line with van Gent and Caires (2011) who concluded that depth limited wave fields propagating over a long horizontal bottom are equally well (or equally bad) described by the deep water Rayleigh and shallow water Battjes and Groenendijk (2000) distributions. In other words, Van Gent and Caires (2011) found that the wave height distribution lies in between the Rayleigh and Battjes and Groenendijk (2000) distribution. This means that after a depth transition the wave height distribution is in accordance with a shallow water distribution. However, after propagation of the wave field over a long horizontal bottom, the distribution is expected to redistribute to Rayleigh. Note that Battjes and Groenendijk (2000) is also only valid for sloping (shallowing) foreshores. Considering the datasets used in this research, all tests contain a horizontal foreshore with a mean distance of 0.4 times the local wave length between the toe and the most nearshore gauge. This distance is most likely to be too short for the shallow water distribution to change its shape. However, this process remains an uncertainty for assessing the relation between the wave height and wave run-up height or front velocity.

3.1.1 Theory of relevant wave height distributions

To check the validity of the obtained wave height exceedance distributions, the data is compared to the deep water Rayleigh distribution (Longuet-Higgins, 1952) and the shallow water distributions of Battjes and Groenendijk (2000) and the newly developed shallow water distribution by Karmpadakis *et al.* (2022). These distributions are further elaborated in this section.

3.1.1.1 Deep water Rayleigh distribution

It is widely accepted to use the Rayleigh distribution to describe short-term wave statistics for waves in deep water. The theory is based on linear wave theory and valid for a wave field with a narrow spectrum. Longuet-Higgins (1952) has shown that for these conditions, wave heights obey the Rayleigh distribution, which is here written as

$$Q(H) = \exp\left[-2\left(\frac{H}{H_{m0}}\right)^2\right] \qquad (3.1)$$

With Q(H) the exceedance probability for a given wave height H and H_{m0} the spectral significant wave height.

3.1.1.2 Shallow water distribution of Karmpadakis *et al.* (2022)

Karmpadakis *et al.* (2022) presents a continuous shallow water wave height distribution based on a large database of experimental simulations of short-crested sea states on horizontal bottoms. The distribution is validated using a large database of field measurements that include short-crested waves. It is, for now, the only distribution to predict wave heights over flat beds. The new distribution is written here as

$$Q(H) = \exp\left[-A\left(\frac{H}{H_{RMS}}\right)^K\right] \qquad (3.2)$$

with H_{RMS} the root-mean-square wave height, A the scale parameter and K the shape parameter. The parameters are written as

$$H_{RMS} = 0.5316\beta H_s - 0.03776, \quad \beta = \sqrt{1-\rho}, \quad \rho = r(T^*), \quad r(\tau) = \frac{\int_0^\infty S(f)\cos(2\pi f\tau)df}{\int_0^\infty S(f)df} \qquad (3.3)$$

$$K = a\exp\left(b\frac{H_{RMS}}{d}\right) + c, \quad A = \left[\Gamma\left(\frac{2}{K}+1\right)\right]^{K/2}, \quad \Gamma(x) = \int_0^\infty t^{x-1}e^{-t}dt \qquad (3.4)$$

With β the degree of de-correlation between wave crests, ρ a non-dimensional parameter following the first minimum of the autocorrelation r(τ=T*) function, S(f) the spectral density function, f the frequency, a, b and c as empirical coefficients, d the water depth and Γ(x) the gamma function.

It is noted that the distance of the fitted wave height distribution and the start of the shallow flat bathymetry is unknown. Also, the laboratory data has been scaled with a factor of $1{:}n_{Fr}$ = 1:100 according to the Froude scaling laws. The parametric fit of the root-mean-square wave height H_{RMS} is therefore derived for $\beta H_s > 2$ with a non-dimensionless constant of -0.03776. This means that the distribution cannot predict the wave heights for small scale experiments without upscaling. For example, for β = 0.7, H_s = 10 m and H_s = 0.1 meter a ratio of H_{RMS}/H_s = 0.37 and -0.005 is found. In this research, the Karmpadakis *et al.* (2022) distribution is therefore derived with upscaling of the data.

3.1.1.3 Shallow water distribution of Battjes and Groenendijk (2000)

The Battjes and Groenendijk (2000) distribution is a composite function of the Rayleigh distribution for lower wave heights and Weibull distribution with exponent 3.6 for the higher wave heights. This distribution is relevant in this context because of its implementation in the COM and Basic Module Grass Outer Slope (in Dutch: ‘Basis Module Gras Buitentalud’). For this reason, this distribution is also considered in this research.

The formulation is derived using laboratory experiments with long-crested JONSWAP wave forcing and with a sloping foreshore with slopes of 1:20 to 1:250. The distribution can be written as follows,

$$Q(H) = \begin{cases} \exp\left(-\dfrac{H^2}{H_1^2}\right) & \text{for} \quad H \le H_{tr} \\ \exp\left(-\dfrac{H^k}{H_{tr}^{k-2} H_1^2}\right) & \text{for} \quad H \ge H_{tr} \end{cases} \tag{3.5}$$

with H_1 the parameter of the Rayleigh distribution, k the Weibull parameter and H_{tr} the transition wave height as a function of the water depth d and sea bed slope α,

$$H_{tr} = (\beta_{tr,1} + \beta_{tr,2} \tan\alpha) \cdot d \tag{3.6}$$

and parameters $\beta_{tr,1}$ $\beta_{tr,2}$. By analysing the laboratory data, Battjes and Groenendijk (2000) determined that $\beta_{tr,1}$ = 0.35, $\beta_{tr,2}$ = 5.8 and k = 3.6. It must be noted that the foreshores of all datasets considered in this research are horizontal bottoms. These infinitely small slopes (<1:250) are not included in the database of Battjes & Groenendijk (2000).

3.2 Deriving the run-up height and front velocities

This section briefly summarises the data handling of the datasets to obtain the run-up and velocity signal. An elaboration of the data handling is given in Deltares (2022a) and in this report attached as Appendix B.

3.2.1 Wave run-up detection

After processing the video footage and the numerical data, the raw wave run-up front signal is smoothened by a 3 point simple moving average. Following, to detect individual wave run-up events, a peak over threshold is applied using a varying threshold of a moving average over two times the spectral wave period $2 \cdot T_{m-1,0}$. The maximum and minimum wave run-up height is found using respective max and min functions. Each event is now identified from a minimum to the next maximum. The run-down, maximum to minimum is ignored.

For overtopping events, when the run-up height exceeds the crest height or measurement range, the maximum run-up height cannot be determined. The run-up height during these events is set as not-a-number (NaN). Note that the maximum front velocity, however, can be derived as the maximum is not expected to occur at the top of the dike.

3.2.2 Derivation of run-up front velocity

The derivative of the wave run-up front signal gives the front velocity in time. The velocity is calculated by central differencing using points i+1 and i-1. It is noted that this leads to some additional smoothing. Following, the acceleration is calculated by similarly, only now taking the second derivative. The acceleration is used to filter unrealistically high accelerations. Subsequently, the maximum velocity is determined over the identified run-up event (not including the run-down). It is noted that the measurement location of the maximum front velocity on the dike slope differs per wave run-up event due to varying wave set-up.

3.3 Scale effects between small- and large-scale physical facilities

The comparison of two sets of Delta Flume 2022 and Scheldt Flume 2018 tests shows that no significant scale effects between small- and large-scale physical model facilities are observed.

The compared experiments have been performed with virtually the same breaker parameter and dimensionless water depth as two small-scale Scheldt Flume 2018 tests. Although the time signal of the surface elevation following a JONSWAP wave spectrum is different, the exceedance distributions should be comparable in case of no scale effects. Figure 3.1 and Figure 3.2 show the wave height, wave run-up and front velocity distribution of a set of Delta Flume and Scheldt Flume tests. Some small deviations can be observed in the right tails of the distributions. This is to be expected due to the events' low probability of occurrence. It is concluded that the distributions overall are very similar, thus no scale effects are observed. It is noted that the wave run-up and velocities are both measured by a video camera.

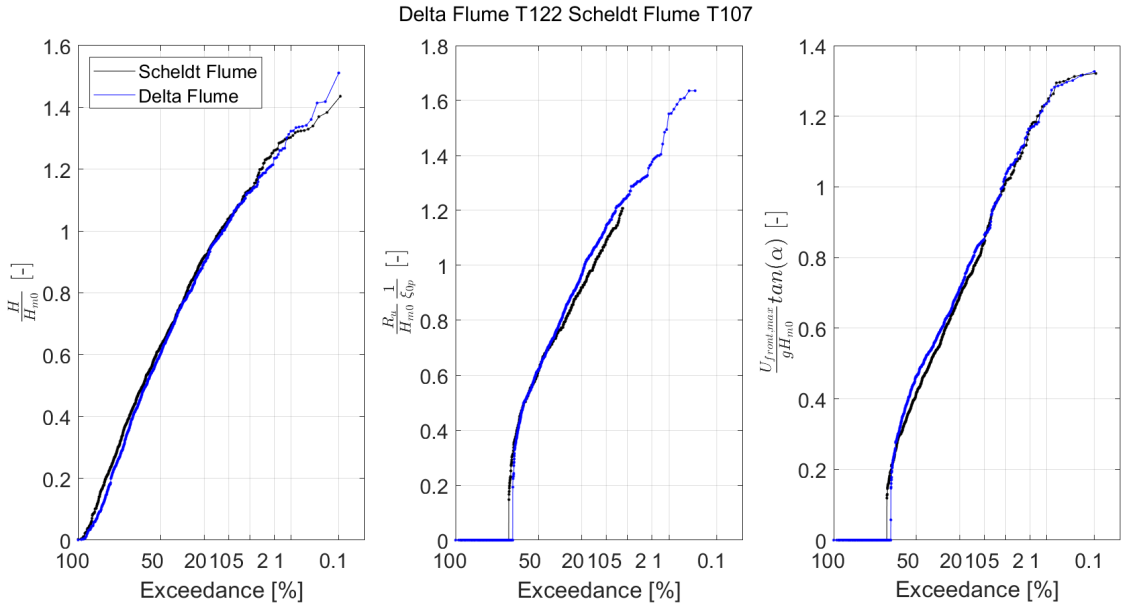

Figure 3.1 Scheldt Flume 2018 test T107 in black and Delta Flume 2022 test T122 in blue with $\xi_{m-1,0}$≈1.9 and H_{m0}/d≈0.33. From left to right: dimensionless wave height, dimensionless run-up height, dimensionless front velocity

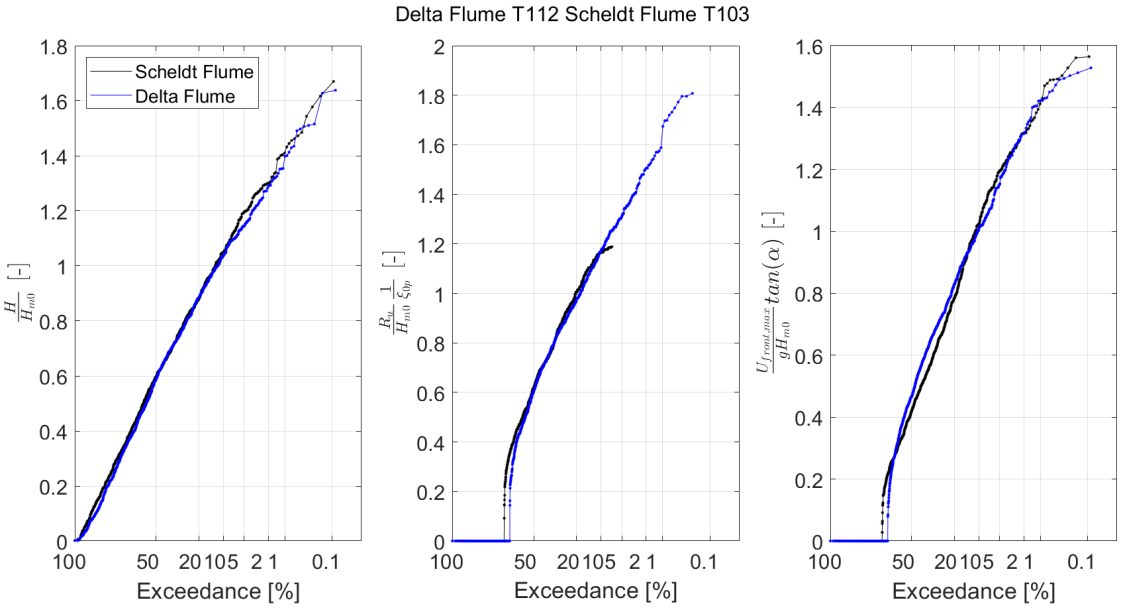

Figure 3.2 Scheldt Flume 2018 test T103 in black and Delta Flume 2022 test T112 in blue with $\xi_{m-1,0}$≈1.9 and H_{m0}/d≈0.25. From left to right: dimensionless wave height, dimensionless run-up height, dimensionless front velocity

4 Assessing the influence of water depth on the wave (run-up) height

This chapter shows that the wave height distribution is in accordance with theory and that the wave run-up distribution for smaller water depths seems to not entirely follow the deflection of the wave height distribution. For deep and shallow water, the wave height distribution is practically equal to Rayleigh and the theoretical (deflected) shallow water distributions respectively. The wave run-up height distribution is not Rayleigh distributed (based on $R_{u2\%}$) in deep and shallow water and, similar to the wave height distribution, (slightly) deflects for shallowing water. The difference with Rayleigh for the wave *run-up* height however is significantly smaller in comparison to the wave height distribution.

This chapter also shows that i) a relation between the wave height distribution and wave *run-up* height distribution cannot be derived with confidence for low exceedance probabilities and ii) cannot be improved by introducing a factor based on the relative water depth. Conclusion i) is caused by a lack of data in the low run-up probabilities as most experimental data is generated with the focus on overtopping. An overview of the wave height versus the wave run-up height distribution does not show a pattern for the relative water depth this leads to conclusion ii).

The chapter is structured as follows. First, the wave height and wave *run-up* height distributions are assessed. Second, the difference of the wave (run-up) height distribution with the (theoretical) Rayleigh distribution is discussed. Last, the relation between the wave height and wave run-up height distribution is assessed by direct comparison. As it is not trivial to link a wave to a wave run-up event, this chapter only considers exceedance distributions of both.

4.1 Wave (run-up) height distribution

Figure 4.1 shows the wave height and wave run-up height exceedance distributions of two Delta Flume 2022 tests. The data is processed in accordance with the methods described in Chapter 3. For both tests, the steepness and breaker parameter are held constant while the relative water depth is varied. For the deep water test, T103, $H_{m0}/d=0.1$ and for the relatively shallow water test, T123, $H_{m0}/d=0.32$. A Rayleigh distribution is drawn using the parameters (H_{m0} and $R_{u2\%}$) of the deep water test T103 for a fair comparison. The left panels, that show the wave height, include the shallow water distributions of Battjes and Groenendijk (2000) and Karmpadakis et al. (2022).

The top panels, test T103 with $H_{m0}/d=0.1$ (deep water), show that the wave height is roughly Rayleigh distributed and that the wave *run-up* height slightly deviates from Rayleigh, with Rayleigh drawn through the $R_{u2\%}$ value. Test T103 is representative for all tests with a relatively large water depth. It is noted that wave run-up with a high exceedance (>60%, left side of the plot) significantly deviates from the other data in the plot as the smallest run-up events are more difficult to detect and can be missed. To tackle this effect the run-up exceedance is derived using the known number of waves and overtopping events (see Chapter 3). This explains the ‘zeros’ at low exceedance probabilities and deviation from Rayleigh at these high exceedance probabilities. The tail of the distribution also deviates from Rayleigh. This is because the tail is based on a very limited number of extreme run-up events which makes it relatively unstable and thus likely to deviate from Rayleigh.

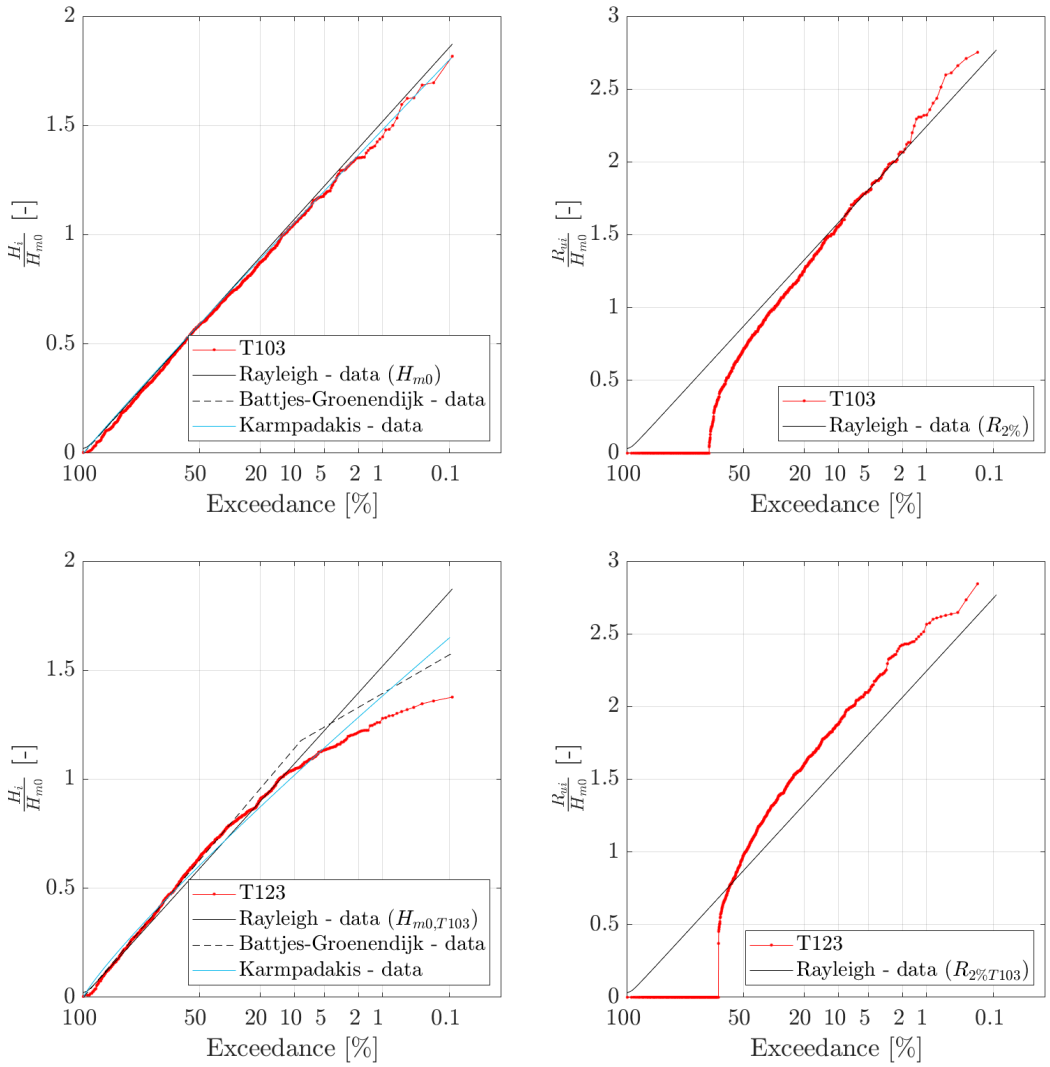

Figure 4.1 Wave height exceedance (left panels) and wave run-up height (right panels) exceedance distributions of Delta Flume 2022 tests with a relative water depth of H_{m0}/d=0.1 (top panels) and H_{m0}/d=0.32 (bottom panels). The steepness ($s_{m-1,0}$) and breaker parameter ($\xi_{m-1,0}$) of both tests equal approximately 4% and 1.36 respectively. The Rayleigh distribution is based on the measured H_{m0} and $R_{u2\%}$ of the relatively deep water test T103.

The bottom panels, test T123 with H_{m0}/d=0.32 (shallow water), show that the wave height clearly deflects from a Rayleigh distribution and that the wave *run-up* height distribution follows this deflection somewhat, although it seems to much a lesser extent. The bottom left panel shows that the wave height in this case is not predicted that well by the 'shallow water' Battjes and Groenendijk (2000) and Karmpadakis *et al.* (2022) distributions. It is noted that for most tests the prediction of the shallow water distribution is better. For most tests, the Battjes and Groenendijk (2000) distribution overestimates the measured wave heights. For some tests, including T123, the Karmpadakis *et al.* (2022) distribution slightly underestimates the waves with high probabilities and overestimates the waves with low probabilities of exceedance. For some tests, the Karmpadakis *et al.* (2022) prediction matches the measured wave heights accurately.

Comparing the wave run-up distributions shown in the bottom right and the top right panel, a deflection similar to the development of deep to shallow wave height distributions can be observed. The deviation from Rayleigh, a deviation from a straight line on Rayleigh axis is however is relatively much smaller than for the wave height. Remarkable is that the deviation

at $R_{u2\%}$, increasing for shallower water, is contradictory to the wave height, decreasing for shallow water. In addition, it is remarkable that the measured normalised wave run-up height (red dots) in shallow water significantly exceed the deep water Rayleigh distribution. The exceedance distributions of test T123 are representative of all tests with a relatively small water depth.

4.2 Comparing the wave (run-up) height with Rayleigh

To further investigate the changing shape of the wave height and wave run-up height distributions due to shallow water effects, the deviation from Rayleigh (following Eq. (3.1) for the wave height and using the $R_{u2\%}$ value for the wave *run-up* height) is assessed for all 47 tests of Data Sets 1-3.

The left panel of Figure 4.2 shows that for smaller water depths (with deep $H_{m0}/d=0.1$ in blue and shallow $H_{m0}/d=0.4$ in red) and low exceedance probabilities (<20%) the difference with a Rayleigh distribution significantly increases. This is in qualitative accordance with the shallow water distributions of Battjes and Groenendijk (2000) and Karmpadakis *et al.* (2022).

The right panel of Figure 4.2 shows that the wave run-up height distribution for deep and shallow water deviates from Rayleigh. For relatively large water depths (blue markers), Rayleigh seems to over- and underestimate the run-up for high and low exceedance probabilities respectively. For relatively small water depths, the opposite seems to be the case. It is noted that wave run-up events with high exceedance probabilities (>60%) are not shown as these are not (accurately) measured. In addition, it is noted that diagonal lines can be observed in the figure. This is an artefact of the step gauge measuring technique used in the numerical Scheldt Flume 2019 dataset. This is because the maximum run-up height in time is in this case a staircase signal due to the height difference of the gauges along the slope. Furthermore, it must be noted that the number of data points for low exceedance probabilities is limited. This is because the numerical and physical Scheldt Flume tests have been performed with the focus on wave overtopping. A significant amount of the waves therefore overtopped the modelled dike. Hence, the wave run-up height of these overtopping events could not be determined.

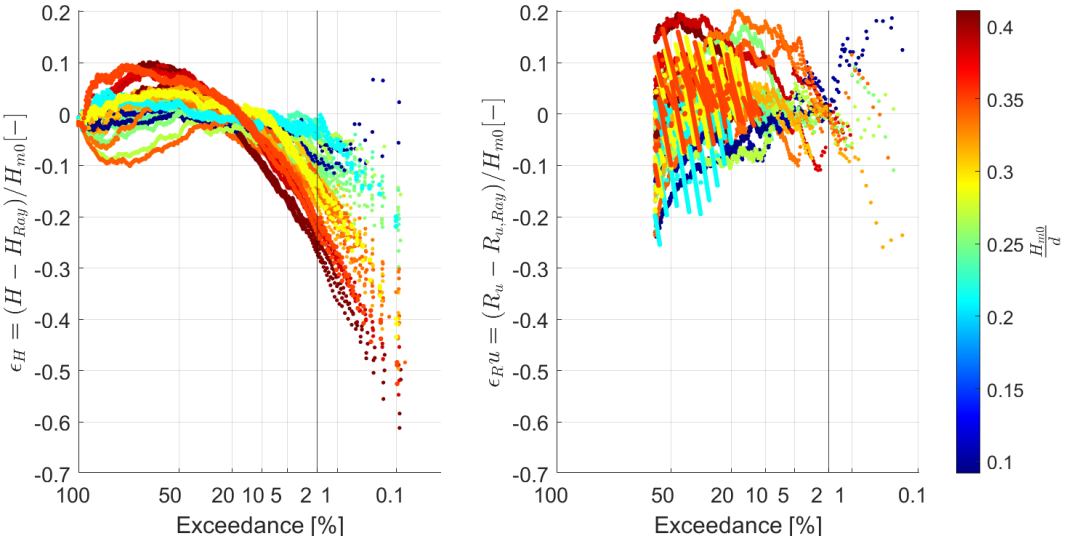

Figure 4.2 Relative difference between the obtained wave height (left) and wave run-up height (right) distribution and theoretical (Eq. (3.1) and $R_{u2\%}$ respectively) Rayleigh distribution. All datasets with varying water depth are shown. The relative water depth is shown in colour with blue a relatively deep, and red a relatively shallow foreshore.

Comparing the left and right panels of Figure 4.2, it can be concluded that the difference, in the tail of the distribution, between Rayleigh and wave *run-up* height distribution is smaller than the difference between Rayleigh and the wave height distribution. Also, for the lowest exceedance probabilities in the wave run-up height distribution no consistent pattern can be observed for different relative water depths. This in contrast to the clear pattern observed for the wave height distribution in the left panel. It must be noted however that the right panel is sensitive for the choice of where the Rayleigh distribution is drawn through. Selecting a lower exceedance probability ($R_{u40\%}$ instead of $R_{u2\%}$) the panel will show a more layered and fanned out picture. It still holds however that the layering is inconsistent. Also, as most wave run-up research and measurements, such as TAW (2002), are performed with a focus on the $R_{u2\%}$, the Rayleigh comparison and its conclusions are drawn using this point of reference.

4.3 Assessing the relation between wave height and wave run-up height

This section directly compares the normalized wave height to the normalized wave *run-up* height to research a relation between the two. To normalize both parameters the research of TAW (2002) is considered. Within the TAW (2002) research, several datasets are analyzed and two empirical formulations to estimate the $R_{u2\%}$ wave run-up height are derived. Eq. (3.7) presents the formulation for breaking waves,

$$\frac{R_{u2\%}}{H_{m0}} = 1.65\gamma_b\gamma_f\gamma_\beta\xi_{m-1,0} \tag{3.7}$$

with a maximum for larger breaker parameters, $\xi_{m-1,0}$, for non-breaking waves:

$$\frac{R_{u2\%}}{H_{m0}} = \gamma_f\gamma_\beta\left(4.0 - \frac{1.5}{\sqrt{\xi_{m-1,0}}}\right) \tag{3.8}$$

With γ empirical factors dependent on the roughness γ_f, angle of wave attack γ_β and the presence of a berm γ_b. It is noted that for the data analyzed in this research, all γ-factors are equal to 1. The TAW (2002) formulations are visualized in Figure 4.3 with all gamma factors equal to 1.

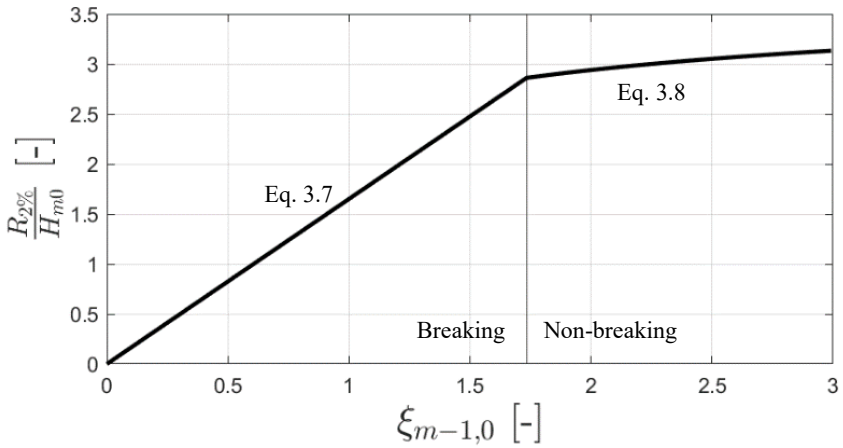

Figure 4.3 Wave run-up height formulations of TAW (2002) with all empirical γ factors equal to 1.

The TAW (2002) formulations show that the wave run-up height for breaking waves is proportional to the breaker parameter and the significant wave height $R_u \propto H_{m0}\xi_{m-1,0}$. For non-breaking waves, proportionality is more difficult to define. As Eq. (3.8) results in almost a linear relation for $\xi_{m-1,0} > 1.73$, it is reasonably assumed that also for non-breaking waves the

proportionality $R_u \propto H_{m0} \xi_{m-1,0}$ holds. However, because there is a clear tipping point between breaking and non-breaking waves, the data is split and analyzed in these two categories. It is noted that the separated plots show the same results as a combined plot. Concluding, the wave run-up height in this research is normalized by the significant wave height and breaker parameter.

4.3.1 Selecting relevant datasets

Section 4.2 has shown that there is limited wave run-up height data due to the focus of most datasets on wave overtopping. In case of overtopping, the maximum wave run-up height cannot be determined. Since the influence of water depth in the wave height distribution only starts to show at low exceedance probabilities (approximately at 12% exceedance for H_{m0}/d = 0.33, which can be estimated by the transitional wave height H_{tr} introduced by Battjes and Groenendijk (2000)), the influence of water depth on the wave *run-up* height is also expected only to show at low probabilities. To properly assess the influence of water depth on the relation between the wave height and wave *run-up* height, only tests that include the relevant range (100% till smaller than H_{tr}% exceedance) in wave run-up should be considered. This is visualized in Figure 4.4. It can be seen that tests that do not include wave run-up height data past the transition wave height H_{tr} (Battjes & Groenendijk, 2000) is excluded.
It is noted that for deep water (H_{m0}/d = 0.1) an exception is made as a deep water Rayleigh distribution is expected.

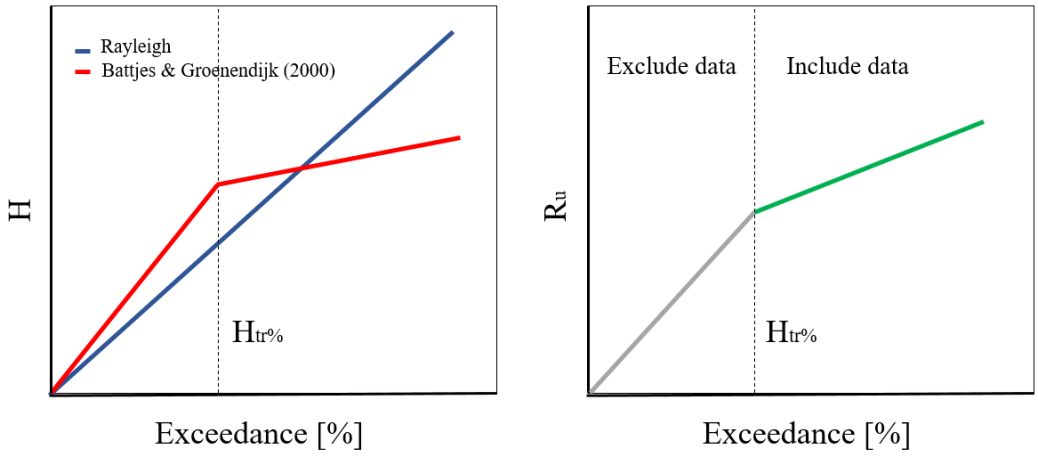

Figure 4.4 Illustration of the selection of relevant datasets. Datasets that do not include wave run-up height data for lower exceedance probabilities than the transition wave height (Battjes & Groenendijk, 2000) are excluded. An exception is made for deep water (H_{m0}/d = 0.1) Rayleigh distributions.

4.3.2 Assessing the relation

Figure 4.5 shows the wave height versus the wave run-up height distribution, where each line represents one test. In this figure, a blue line represents relatively deep water (i.e H_{m0}/d = 0.1) and a red line represents relatively shallow water (i.e. H_{m0}/d = 0.4) at the toe of the dike. All tests with breaking and non-breaking waves are shown in two separate panels. It is noted that as it is not possible to link a wave to a wave run-up event, only a relation between the exceedance distributions is investigated, i.e. the $H_{p\%}$ is plotted against the $R_{u,p\%}$, with *p* the percentage of exceedance. This means that the $R_{u5\%}$ wave run-up height is not necessarily the result of the wave height with a 5% exceedance probability. The data on the x- and y-axis are thus not the same events. The left panel of Figure 4.5 includes the estimation of TAW (2002). The $R_{u2\%,TAW}/(H_{m0}\xi_{m-1,0})$ = 1.65 (See Eq. (3.7)) is plotted against the 2-percent wave height in accordance with Rayleigh $H_{2\%}/H_{m0}$ = 1.4. In this figure the TAW (2002) estimation therefore assumes Rayleigh distributed wave run-up heights. The TAW (2002) prediction for non-breaking waves is ambiguous and is therefore not included.

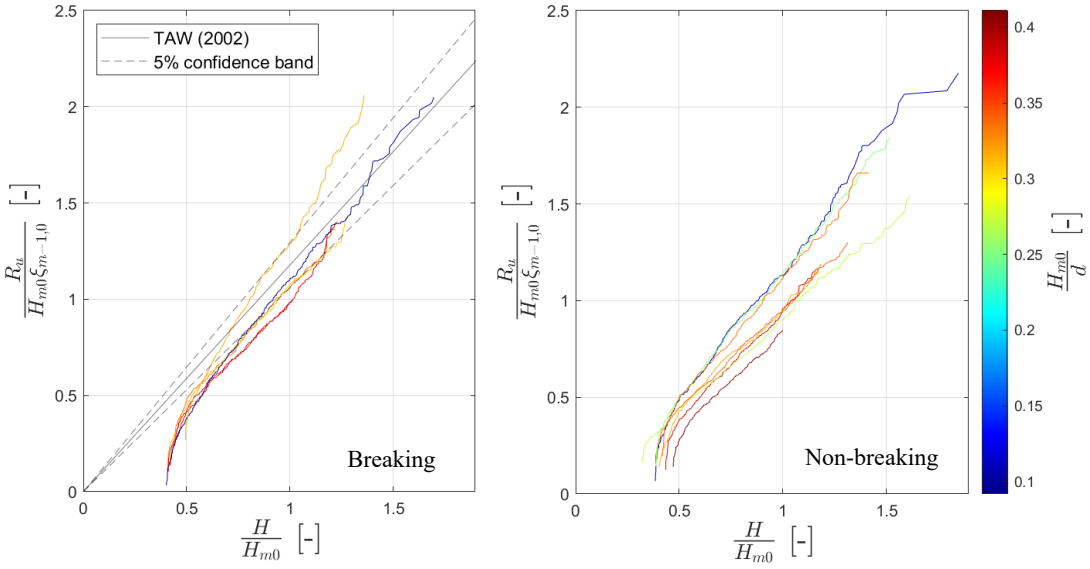

Figure 4.5 The normalised measured wave run-up height (y-axis) exceedance distribution versus the normalised measured wave height (x-axis) exceedance distribution for the selected tests with breaking waves (left panel) and non-breaking waves (right panel). The relative water depth is shown in colour with blue a relatively deep, and red a relatively shallow foreshore. In the left panel the TAW (2002) prediction including the 5% confidence band is shown.

Figure 4.5 shows that the breaking waves are in accordance with the TAW (2002) run-up formulation. In addition, the lines in Figure 4.5 are not completely straight for all 11 (out of 47) tests, suggesting that there is not a simple linear relation between the wave *run-up* height distribution and wave height distribution. This is in accordance with the observations from Figure 4.1 and Figure 4.2 as the deviation from Rayleigh seems to be less for wave run-up height than for the wave height. If we take a closer look at the higher waves with low exceedance probabilities (right side of Figure 4.5), the lines start to deviate from a simple linear relation. This last part of the line is most important in the context of the COM as these represent the run-up events with low exceedance probabilities (high run-up and relatively high velocities). A significant part of this data is missing as most of the tests have been performed within overtopping research and therefore lack information on the maximum run-up height for the highest run-up events. Therefore, one cannot confidently derive a relation that holds for low exceedance probabilities based on this data set. For higher exceedance probabilities (left side), a linear relation can be identified between the wave height and wave *run-up* height. In Appendix C an overview with all 47 tests is shown.

No factor for the relative water depth can be derived to improve the general relation between the wave run-up and wave height distribution. Figure 4.5 shows that the lines of all tests are quite fanned out. This means that the use of a factor, such as the slope or wave steepness, on the wave height, could ensure that the lines get closer together. If all lines lie on top of each other, this indicates a strong relation without much uncertainty. As the colors, which represent the depth, are not displaying a clear pattern, no factor for the relative water depth can be derived that explains a significant part of the observed variance. It is noted that a factor for the relative water depth is also sought in combination with other factors, such as the foreshore. With the application of other factors, still no clear pattern in relative water depth is observed.

5 Influence of water depth on the front velocity

This chapter demonstrates that the front velocity distribution is not Rayleigh distributed for shallow and deep water wave forcing. In addition, it shows that there seems to be a stronger link between the wave *run-up* height and front velocity distributions than between the wave height and front velocity distributions. This is convenient as most research is based on typical $R_{u2\%}$ wave run-up heights (TAW, 2002). Last, it shows that the relation between the wave run-up height and front velocity distribution cannot be improved by a factor based on the relative water depth.

The chapter is structured as follows. First, the influence of a varying relative water depth on the wave height and front velocity exceedance distributions is assessed. This section only considers exceedance distributions as it is not trivial to link incoming waves to velocities resulting from wave run-up events. In addition, the influence of water depth on the relation between the wave run-up height and front velocity is assessed. The last section of this chapter ends with a summary of the conclusions.

5.1 Assessing the wave height and front velocity distribution

Figure 5.1 shows the measured wave height and measured maximum front velocity distributions of a relatively deep and relatively shallow Delta Flume test. It is noted that the measurement location of the maximum front velocity on the dike slope differs per wave run-up event due to varying wave set-up. As the wave height distribution is discussed in Section 4.1, this section focusses on the front velocity distribution and its relation to the wave height distribution.

The velocity distributions, based on the maximum front velocity per wave run-up event and shown in the right panels of Figure 5.1, are not entirely well described by the Rayleigh distribution. It can be seen that the distributions are approximately linear (Rayleigh) between 60% and 5% exceedance probabilities. For lower exceedance probabilities, both distributions start to deviate from Rayleigh[1]. Furthermore, Figure 5.1 shows that the shape/curvature of the measured velocity distributions is quite similar. Comparing the velocity distribution of the deep water test, T103 with $H_{m0}/d = 0.1$, to the shallow water test, T123 with $H_{m0}/d = 0.32$, the latter contains significantly larger normalised front velocities. This is not in line with the shallow water (deflected) wave height distribution. It is therefore expected that no clear relation is to be found between the wave height (incoming wave field) and front velocity distribution. It is noted that the breaker parameter and the wave steepness during test T103 and T123 are similar. The Rayleigh distribution plotted in the front velocity exceedance distribution is based on the $U_{2\%}$ of the deep water test. Also, it is noted that unlike the wave run-up height, the front velocity distribution can be derived for overtopping events. As the maximum front velocities are expected to occur before the front reaches the crest, the front velocity can be derived. Furthermore, it is noted that the normalised and thus not the absolute velocities are shown. The absolute front velocities of test T123 are most likely smaller than deep water test T103, because the denominator is smaller due to wave breaking on the shallow foreshore. Last, it is noted that the deep and shallow water test are representative for all datasets.

[1] The right tail of the front velocity distribution (the highest velocities) depends on the data analysis method used. To eliminate unphysically large velocities, a maximum acceleration factor is determined. This flattens the tail of the velocity distribution as extreme velocities are removed. The tail is thus a balance between removing measurement errors and saving “true” velocity measurements.

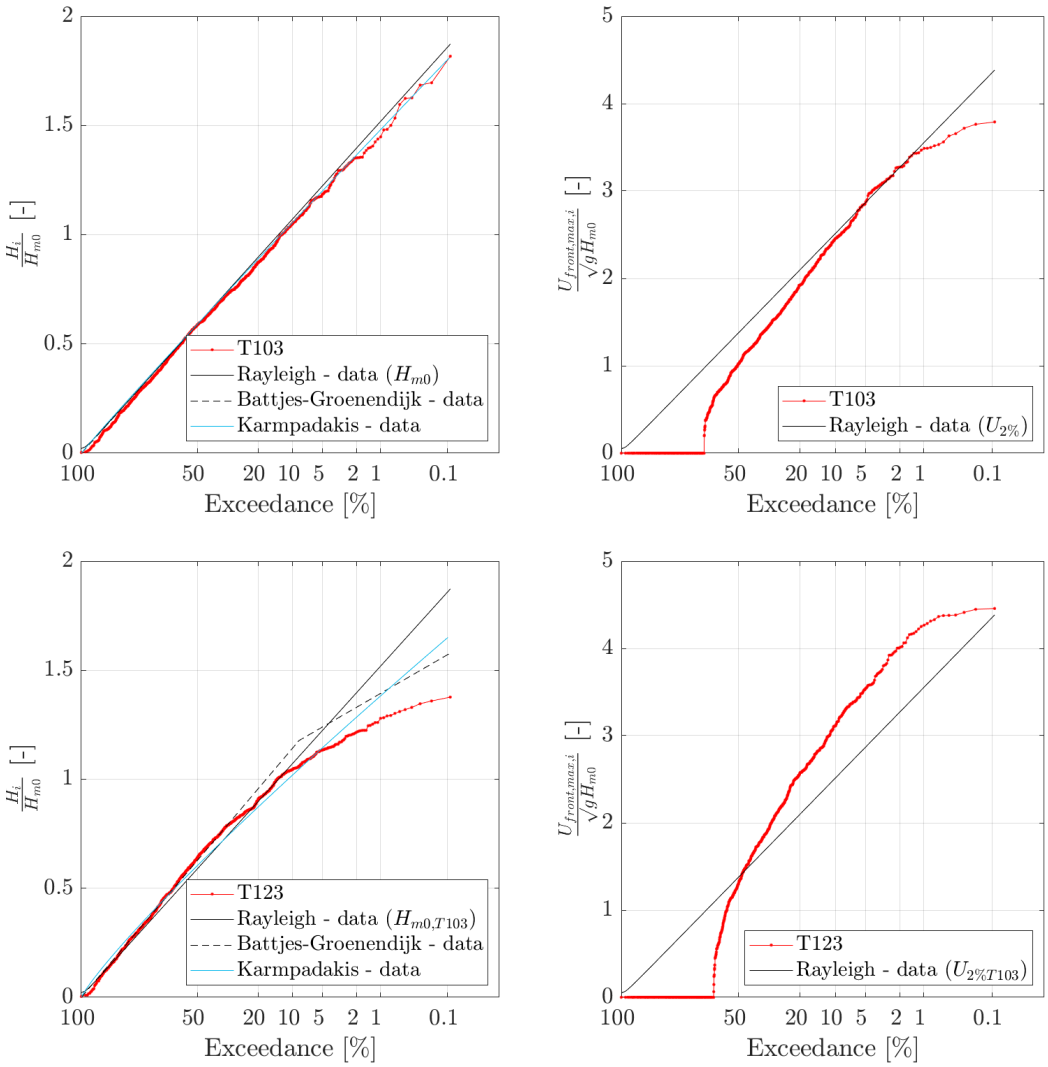

Figure 5.1 Wave height exceedance (left panels) and front velocity (right panels) exceedance distributions of Delta Flume 2022 tests with a relative water depth of $H_{m0}/d=0.1$ (top panels) and $H_{m0}/d=0.32$ (bottom panels). The steepness ($s_{m-1,0}$) and breaker parameter ($\xi_{m-1,0}$) of both tests equal approximately 4% and 1.36 respectively. The Rayleigh distribution is based on the measured H_{m0} and $U_{u2\%}$ of the relatively deep water test T103

To further investigate the relation between the wave height distribution, the wave height is plotted versus the velocity distribution. In order to properly assess the influence of water depth, other dominant processes must be eliminated by correct normalisation. To normalize the front velocity the law of energy conservation and the research of TAW (2002) is considered. Energy conservation in this case means that the total amount of kinetic energy, $E_{kin} = \frac{1}{2}mu^2$, should equal the amount of potential energy, $E_{pot} = mgh$. With m the mass, g the gravitational acceleration, u the front velocity and h the height difference on the slope, thus the run-up height. The front velocity is therefore proportional to the square root of the wave run-up height and gravitational acceleration. Combining this with the wave run-up formulations derived by TAW (2002), see Section 4.3, the front velocity is found to be proportional to $U_{front} \propto \sqrt{(gH_{m0}\xi_{m-1,0})}$. The effects of different breaker types on the slope is therefore accounted for. It is noted that again the breaking and non-breaking waves are separately analyzed. In addition, it is noted that in both cases the same results are found.

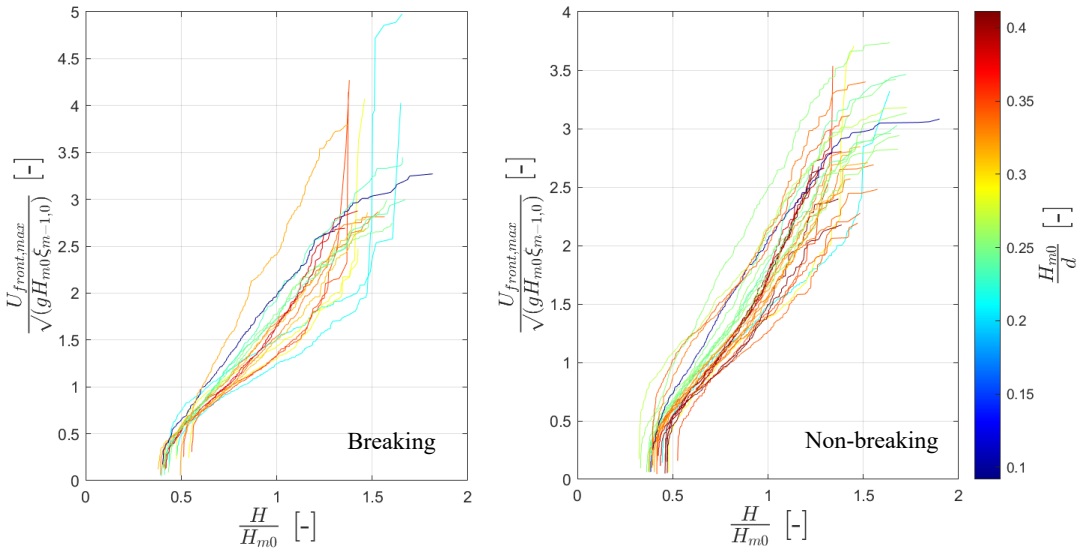

Figure 5.2 The normalised measured front velocity (y-axis) versus the normalised measured wave height (x-axis) exceedance distribution for breaking (left panel) and non-breaking (right panel) waves. The relative water depth is shown in colour with blue a relatively deep, and red a relatively shallow foreshore.

The relation between the wave height and front velocity exceedance distribution is plotted in Figure 5.2. As expected, the lines (each one representing one test with blue relatively deep and red relatively shallow foreshores) are not straight and thus no linear relation is identified. Furthermore, Figure 5.2 shows that no factor or trend can be identified for the relative water depths. Clearly, no pattern in the water depths is observed.

Comparing Figure 5.2 with Figure 4.5, it is concluded that the relation between the wave height and wave run-up height seems to be stronger than the relation between the wave height and front velocities. This is because the lines in the plot of the wave height versus the wave run-up height in Figure 4.5 are straighter and lie much more on top of each other (less variance) than the lines in the plot of the wave height versus the front velocity (Figure 5.2).

5.2 Investigating the relation between the wave run-up height and front velocity

This section assesses the influence of water depth on the relation between the wave run-up height and maximum front velocity per wave run-up event. To properly compare both parameters, the wave run-up height and front velocity are normalised by the significant wave height and breaker parameter. This is in accordance with the law of energy conservation and the research of TAW (2002). As a wave run-up event is linked to the maximum front velocity of that event, both the distributions $U_{p\%}$ and $R_{up\%}$ and the individual events U_i and R_{ui} will be elaborated, with *p* the exceedance probabilities and *i* the index of an event. Both methods are discussed as these are also both considered in the overarching research of Deltares (2022a). The difference between both methods is shown in Figure 5.3.

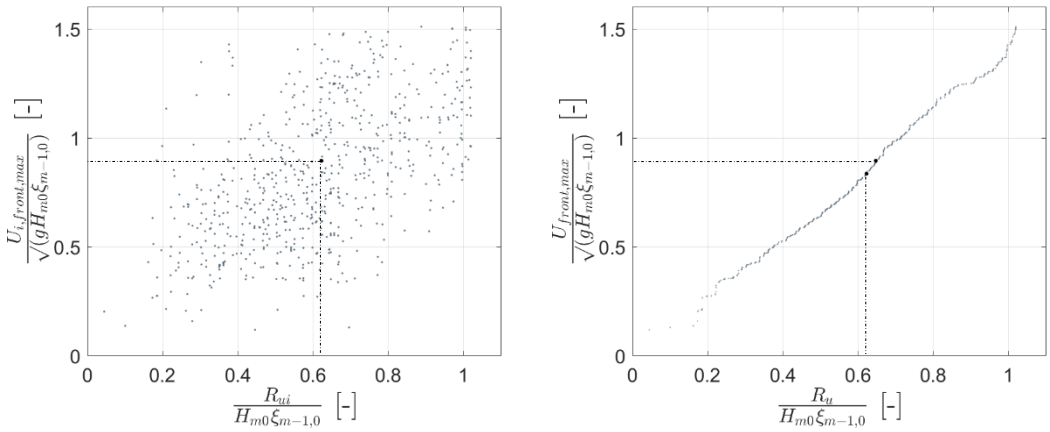

Figure 5.3 Event-based versus the exceedance probability method to assess the relation between the wave run-up height and front velocity. Both figures show the results of one Scheldt Flume 2018, Data Set 1.

The left panel of Figure 5.3 shows the wave run-up height and velocity of event *i* = 150 highlighted in black. Each dot in the plot represents one wave run-up event. In the right panel, event *i* = 150 corresponds with exceedance probabilities of 62% and 66% for the wave run-up height and front velocity respectively. Note the significant scatter in the left panel versus the exceedance distributions in the right panel. This is due to the dependency of the event-based method on the surface elevation timeseries. The wave run-up and velocity are therefore dependent on the wave(s) preceding the considered event. Because it is difficult to assess the influence of water depth with significant scatter, the influence of water depth in the remainder of this report is assessed by the distribution method. For completeness, the event-based method is included in Appendix D but is not further discussed in this report.

5.2.1 Exceedance distribution comparison

Figure 5.4 shows the front velocity and wave run-up height distribution. Each coloured line represents one test with blue a relatively deep and red a relatively shallow foreshore.

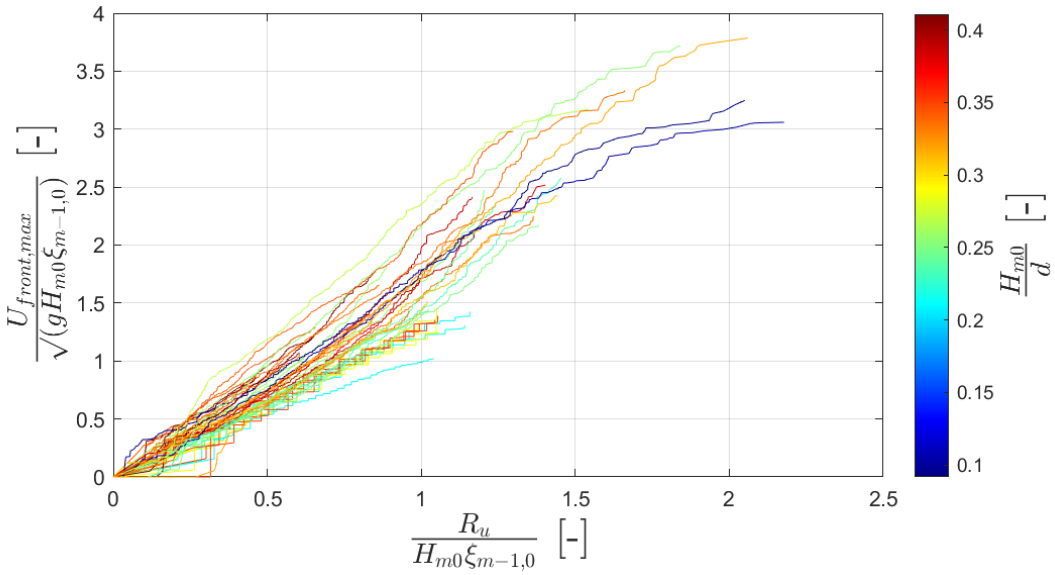

Figure 5.4 The normalised measured front velocity (y-axis) versus the normalised measured wave run-up height (x-axis) exceedance distribution for all tests. The relative water depth is shown in colour with blue a relatively deep, and red a relatively shallow foreshore.

Figure 5.4 and Figure 5.2 show that the front velocity distribution is better linked to the wave *run-up* height than the wave height distribution. Namely, the lines in Figure 5.4 are straighter (which indicates a linear relation) and lie more on top of each other (less variance) in

comparison with Figure 5.2. Considering the latter, it is suggested to derive the front velocities using the wave run-up and not directly from the wave height in case of an accurate estimation of the wave run-up height.

The mix of coloured lines in Figure 5.4 shows that no additional trend in relative water depth can be identified in the relation between the wave run-up height and front velocity. If a trend is present, a factor can be derived to improve the relation of, in this case, the wave run-up height and front velocity. It is noted that the influence of comparing three datasets at once is eliminated by generating and analysing the same figure for each of the three datasets separately. The figures, attached in Appendix D, show that for the three separate datasets, also no trend can be observed. It is noted that the three datasets are also analysed for breaking and non-breaking waves (TAW, 2002). Also in this case, no trend is identified for the relative water depth.

6 Infra-gravity waves in the context of the COM

This chapter discusses the recent research of Lashley (2021) and infra-gravity (IG) waves within the context of the Cumulative Overload Method (COM / Cumulatieve Overbelasting Methode). As IG waves, explained below, become more important in the case of ascending, shallow foreshores, it is considered as a relevant element within this influence of water depth research. In addition, Lashley (2021) shows that IG waves can have a significant negative impact on the safety of Dutch flood defences.

Infra-gravity waves or so-called surf-beat are long period (low-frequency) waves forced by sea and swell waves. The bound waves have a typical period of 25 - 250 seconds, being the scale of the wave groups under the carries sea and swell waves and therefore exist within a typical frequency range of 0.004 - 0.04 Hz or approximately seven times the peak period. For gently-sloping foreshores, the amplitudes of the bound waves increase. In the breaker zone, the IG waves are released as the wave groups cease to exist. Subsequently, the free low-frequency waves propagate towards the shore. For relatively steep sloping foreshores, IG waves are generated by the variation of the location of wave breaking in a cross-section. Higher amplitude wave groups break further offshore than lower amplitude wave groups. These fluctuations result in a set-up and set-down that produce IG waves propagating in on- and offshore direction. Besides the IG waves arising from the existence of wave groups, ‘free’ IG waves or so-called leaky or edge waves are generated from distant sources. (Lashley, 2021)

6.1 Relevant findings of Lashley (2021)

With the focus on wave overtopping, Lashley (2021) studied the impact of IG waves on the probability of failure of flood defences. He proposes two empirical methods to include IG waves; a combination of numerical (SWAN) and empirical (proposed by himself and EurOtop, 2018) models, and an alternative approach that is based entirely on deep water characteristics, the foreshore slope and relative water depth at the structure toe. It is found that the presence of IG waves has a negative (higher than expected amount of overtopping discharge) influence on the safety of flood defences. Shallow foreshores, however, are found to still have a net positive effect on the magnitude of overtopping as wave breaking still results in smaller wave heights.

To quantify the impact of IG waves on the overtopping discharge Lashley (2022) stresses the use of appropriate methods. An appropriate formulation should only be used in their validity range and should be derived for shallow foreshores, where IG waves are relevant.

Lashley (2021) concludes that it is difficult to obtain accurate estimates of wave parameters at the toe of the structure. For this reason, he proposes a new method to derive the shallow water parameters. This consists of a newly developed linear relation between the deep and shallow water wave height.

6.2 Relation to the COM

The research in this report does account for the effect of IG waves. This is because a narrow banded spectrum, which results in wave groups, is generated by the wave board during all tests. In the breaker zone, in shallow water, the IG waves are released as the wave groups cease to exist. Figure 6.1 shows that the spectral density at low frequencies is higher for experiments with shallow foreshores (in red) than for similar tests with deep foreshores (in blue). It is noted that free IG waves are not considered in this and the research of Lashley (2021).

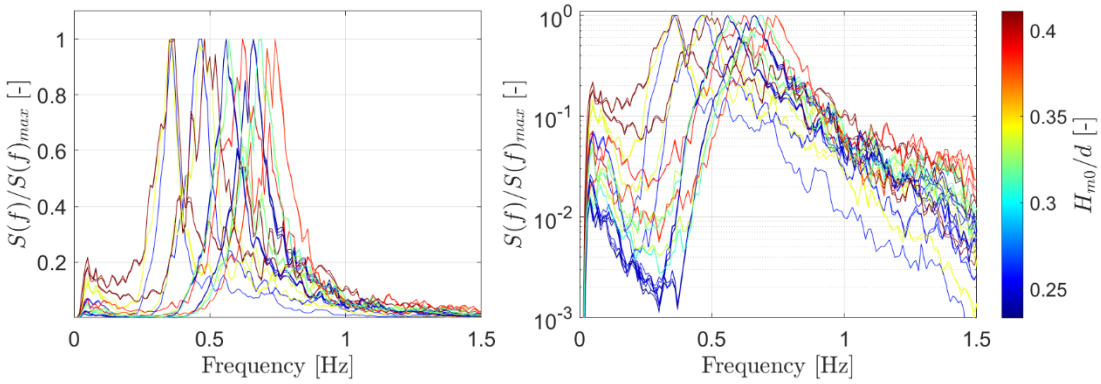

Figure 6.1 Relative spectral density for the Scheldt Flume 2018 experiments measured near the toe of the structure. The relative water depth is shown in colour with blue relatively deep and red relatively shallow water. The left panel shows the spectra with a linear scale. The right panel shows the same spectra with a log scale to zoom in on the low frequencies.

It is shown that the datasets in this research and in Deltares (2022a) contain IG waves arising from wave groups. Free IG waves are not included in the data as these are not forced by the wave board. The impact of excluding these free waves is yet unknown.

Lashley (2021) proposes a new method to derive the shallow water wave parameters using the deep water wave conditions. The new method consists of an empirical linear relation to estimate the significant wave height at the toe, $H_{m0,toe,}$ and a new overtopping formulation. Lashley (2021) notes that the wave period $T_{m-1,0,toe}$ can easily be modelled with existent empirical formulations and its deep water counterpart. As the new velocity formulation requires the wave forcing (i.e. significant wave height) as input (Deltares, 2022a), this formulation could be considered within the context of the COM. It is noted however that for complex situations, such as the Wadden Sea, it is difficult to accurately determine the offshore wave conditions. In addition, it is questioned whether the influence of wave growth due to wind forcing can be included accurately. The possible application area is therefore limited.

7 Discussion

This chapter summarizes the most important points of discussion and limitations of this research.

- There is a lack of wave run-up data in the low exceedance probabilities. This makes it difficult to draw a firm conclusion on the development of the wave run-up height distribution in deep to shallow water and to derive its relation with the wave height distribution.
- There is no accepted formulation to derive the wave run-up height (and front velocity) distribution. It is therefore not possible to check the results of the processing methods used with existing research. Furthermore, comparison with theory, such as the deviation from Rayleigh using $R_{u2\%}$, is perhaps ambiguous but is considered the best available method due to a lack of alternatives.
- All analyzed datasets are generated in 1D physical and numerical wave flumes. This means that only long crested, normally incident waves and no effects in cross-shore variation are included in the data. The conclusions in this research are therefore only valid for 1D situations. It is noted that extensive research has been performed on the (shallow water) wave height distribution and can be predicted accurately for field cases, which per definition include short crested, directional waves and spatially varying bathymetry (Karmpadakis et al., 2022). The effect of the three factors (arising from 1D versus 3D) in combination with influence of water depth on the wave run-up height and front velocities remains however unknown.
- The wave height exceedance distribution of test T123 with $H_{m0}/d = 0.32$ shown in Chapter 4 is not predicted accurately by the Battjes and Groenendijk (2000) or Karmpadakis *et al.* (2022) distributions. For most tests, the Battjes and Groenendijk (2000) prediction overestimates the measured wave heights. For some tests the Karmpadakis *et al.* (2022) distribution underestimates the waves with high probabilities and overestimates the waves with low probabilities. For some tests, the Karmpadakis *et al.* (2022) prediction matches the measured wave heights accurately. As the Battjes and Groenendijk (2000) wave height distribution was derived for sloping foreshores, it was expected that the measurement of the datasets considered in this research with flat beds could differ. The Karmpadakis *et al.* (2022) distribution is calibrated on short-crested sea states on flat bed bathymetries. Considering the bathymetry, logically, Karmpadakis *et al.* (2022) is in better accordance with the datasets considered in this research. The remaining difference between the datasets considered and theory is hypothesized to be due to short- versus long-crestedness. The selection of the most accurate theoretical shallow water distribution thus depends on the situation to be modelled. Another noteworthy observation of test T123 shown in Chapter 4 is that the prediction of both theoretical shallow water distributions differ quite a bit. Generally, this difference is the largest at the transitional wave height (Battjes & Groenendijk, 2000), where Battjes and Groenendijk (2000) predict higher waves than Karmpadakis *et al.* (2022). The difference in wave height prediction at the right tail, at 0.1% probability, seems to be limited (10%).
- The datasets in this research do not include berms and only contain smooth slopes. It is expected that for rough slopes and/or berms the influence of water depth on the maximum wave run-up height is still visible as the wave forcing, which is direct input for R_u, is different for deep (Rayleigh) and shallow water (shallow water distribution). It is unknown if the presence of a berm and/or roughness can impact the degree of influence of water depth (deviation from Rayleigh) on the wave run-up height distribution. The impact of roughness and/or berms on the relations between the wave

height, wave run-up height and velocity distributions is unknown. Also, it is unknown if including one of the three aspects would result in a trend, layering for relative water depths, which is not shown for a 1D structure without a berm and with a smooth slope.The wave height is measured at a small distance offshore of the dike toe on a shallow flat bed. It is unknown if/how quickly the shallow water wave height distribution converges back to a Rayleigh distribution over horizontal bottoms. This process remains an uncertainty in the assessment of the relation between the wave height and wave run-up height or front velocity.

- This research assesses the effect of shallow foreshores using the relative water depth defined as H_{m0}/d. The influence of water depth or non-linearity can also be quantified as a function of kd, with k the wave number and d the water depth, and the Ursell number, which is a function of the wave height (H), wavelength (L) and water depth ($U_r = HL^2/d^3$). These other two approaches can be considered in further research.
- Finding trends and relationships in the available data sets is challenging. In this research the normalization of the wave run-up height is based on the TAW (2002) wave run-up height formulation. The normalization of the front velocity is based on the law of energy conservation. The investigated parameters include the significant wave height, the maximum wave run-up height and the maximum front velocity per wave run-up event. Other choices can be made with respect to normalization and selected parameters.
- The physical and numerical datasets only include bound infra-gravity waves due to the presence of wave groups. ‘Free’ infra-gravity waves, incoming from distant sources, are not included. It is not expected that the inclusion of these free infra-gravity waves will impact the conclusions in this research as these are present in situations with both relatively shallow and deep water conditions.
- Lashley (2021) proposes a new method to derive the shallow water wave parameters using the deep water wave conditions to include the effect of infra-gravity waves. A linear empirical relation is used to determine the significant wave height at the toe, $H_{m0,toe,}$. The wave period $T_{m-1,0,toe}$ is determined using an existent empirical formulations and its deep water counterpart. These parameters could be used in the COM. It is noted however that for complex situations, such as the Wadden Sea, it is difficult to accurately determine the offshore wave conditions. In addition, it is questioned if the influence of wave growth due to wind forcing can be included accurately. The possible application area of the proposed method by Lashley (2021) is therefore limited.

8 Conclusions

This report researches the influence of water depth on the wave height, wave run-up height and maximum front velocity per wave run-up event using available experimental data. Three datasets that have been generated in physical and numerical wave flumes are investigated. The datasets include tests with horizontal beds, smooth slopes and normally incident long-crested waves. This chapter presents the conclusions. First, the research questions are answered. Second, other relevant conclusions are listed.

Can the influence of water depth on the wave run-up height and front velocity be accounted for in the COM?

The influence of water depth cannot (yet) be accounted for in the Cumulative Overload Method (COM). The reason for this is twofold. Firstly, the wave run-up height distribution seems to not entirely follow the wave height distribution. The front velocity distribution does not seem to follow the wave height distribution. Therefore, it cannot simply be assumed that the wave run-up height and front velocity distributions follow the theoretical shallow water wave height distribution. If for example Battjes and Groenendijk (2000) would be used, it is expected that the front velocities are underestimated. Secondly, no relations are available to derive the distribution from one another and the available data is too limited to derive such relations. Important limitations of available datasets stem from the focus of previous research on the wave overtopping discharge (q) while the focus parameter within the framework of the COM is the front velocity (U_{front}).

What is the influence of water depth on the wave height and wave run-up height distribution?

- The wave height distributions of the datasets considered are in accordance with theory. For deep water the wave height distribution is roughly Rayleigh distributed. For shallow water the wave height distribution is in reasonable accordance with the shallow water distributions of Battjes and Groenendijk (2000) and Karmpadakis *et al.* (2022). It is noted that for some cases there is quite a difference between both theoretical distributions. Also, for some cases the measured wave heights differ from both theoretical distributions, see Figure 4.1. It is expected that this difference is due to comparing the theoretical distribution in a non-validated situation (Battjes and Groenenwijk (2000) is not valid for flat beds and Karmpadakis *et al.* (2022) is not valid for long-crested waves).
- For smaller water depths, the wave *run-up* height distribution seems to not entirely follow the development of the wave height distribution. In deep water the wave run-up height exceedance distribution is a relative straight line on a Rayleigh x-axis. In shallow water, the right tail of the wave run-up height distribution flattens.
- The wave *run-up* height distribution deviates significantly less from Rayleigh (based on $R_{u2\%}$) for shallow water conditions than the wave height distribution (based on Rayleigh following Longuet-Higgins (1952)).

How does this influence affect the front velocity distribution?

- The front velocity distribution, based on the maximum front velocity per wave run-up event, for deep and shallow water is not entirely Rayleigh distributed (based on $U_{2\%}$). It is noted that the front velocity distribution is most sensitive to the processing methods used.
- The shape of the front velocity distribution ($U_{front,max}$) does not seem to depend on the relative water depth. Note that this is the case for the wave height and (less significantly) for the wave run-up height distribution. This observation is in accordance

with Deltares (2019) where the overtopping volume distribution was not found to be different for varying relative water depths.

- The relation between the front velocity and wave *run-up* height distribution is stronger than the relation between the front velocity and the wave height distribution. The former relation could be modelled reasonably well, although there is quite some scatter. That the former relation is stronger than the latter could be due to the wave run-up height and velocity distribution being dependent on the wave height time series. The wave run-down of wave 1 can influence the wave run-up of wave 2.

The relative water depth therefore strongly influences the shape of the wave height distribution, to a lesser extent the shape of the wave run-up height distribution and does not influence the shape of the front velocity distribution. It is noted that since previous research (van Steeg et al, 2020) pointed at a significant influence of water depth on wave runup and overtopping, it is recommended to investigate alternative normalization methods to be able to assess the influence of water depth on the scaling of the wave run-up height and velocity distributions, besides the shape aspects that were already investigated in this report.

This research also concludes that a relation between the wave height and wave *run-up* height distribution cannot be derived with confidence based on the available datasets. This is because most tests of the three datasets are generated with focus on the wave overtopping discharge (q). Thus, there is a lack of data in the low exceedance probabilities. The wave run-up height with low exceedance probabilities is important in the context of the COM.

Furthermore, based on the available data, the relations between the wave height and wave *run-up* height distribution, and wave *run-up* height and front velocity distribution seem to be unrelated to the relative water depth, besides the reduced significant wave height due to wave breaking. It is noted that the uncertainty in this conclusion is due to the lack of wave run-up data in the low exceedance probabilities. Also it is noted that this conclusion holds for the *relation* between the parameters. It is shown that the wave height and wave run-up height distributions deviate for varying water depths.

9 Recommendations

This chapter lists the recommendations for further research in two categories.

Recommendations for experimental and theoretical research

- It is recommended to further investigate the relation between the wave height, wave run-up height and front velocities by using (or creating) datasets with 'infinite' long slopes so the tail of the exceedance curves can be determined properly.
- It is recommended to consider additional research into the development of the shallow water wave height distribution over long flat bathymetries. This development is relevant in areas with shallow flat beds such as the Wadden Sea, floodplains and lakes, such as the IJsselmeer. In the context of the COM, this research is required to accurately determine a relation between the wave height and wave run-up height as it is not possible to measure the wave height exceedance distribution directly at the position of the toe while the structure is present.
- It is recommended to physically (laboratory or field measurements) and numerically research the influence of roughness, berms, cross-shore variations, short- and long-crestedness and oblique wave attack on the influence of water depth on the wave run-up height and front velocities. It is however questioned if the influence of water depth would be significantly different in comparison with the datasets considered in this research as the wave forcing in all cases will depend on the water depth and is direct input for the wave run-up height and velocities. On the contrary, the limited water depth could reduce highest, most impactful, waves which are than more effectively reduced by roughness and berms.
- It is recommended to further investigate the influence of the wave shape (flat trough, sharp-crest) on the wave run-up height and velocity distribution. In addition, the influence of the Rayleigh reference line (in this research based on the 2% value) and normalization parameters (in this research based on TAW (2002) and law of energy conservation) are recommended to be researched. This is all the more important because part of the trends reported in this study seemed somewhat ambiguous and can enable direct comparison of the distributions with varying relative water depths. For normalising, one could also investigate individual wave characteristics, such as the wave period. Last, other descriptions of the relative water depth, such as kd, with k the wave number and d the water depth and Ursell ($U_r = HL^2/d^3$), with H the wave height and L the wave length, should be investigated.
- It is recommended to systematically compare the datasets to the theoretical shallow water distributions of Battjes and Groenendijk (2000), derived using long-crested laboratory measurements, and Karmpadakis *et al.* (2022), derived using short-crested field measurements. This will give insights in the performance of both methods for the datasets considered and their possible areas of application.

Recommendation for COM implementation

- For wave height predictions on shallow foreshores it is recommended to select a theoretical shallow wave height distribution with most similarities to the case considered. If a theoretical distribution is used for unvalidated situations (such as flat beds in case of the Battjes and Groenendijk (2000) distribution which is derived for sloping beds) differences between theory and practice is expected.
- Lashley (2021) proposes a new method to derive the shallow water wave parameters using the deep water wave conditions. In this new approach the influence of infra-gravity waves is accounted for. As the new velocity formulation requires the wave forcing (i.e. significant wave height) as input (Deltares, 2022a), this formulation could

be considered within the context of the COM. It is noted however that the application area is limited as for complex situations, such as the Wadden Sea, it is difficult to accurately determine the offshore wave conditions. In addition, it is questioned if the influence of wave growth due to wind forcing can be included accurately.

References

Battjes, J. A., & Groenendijk, H. W., 2000. Wave height distributions on shallow foreshores. *Coastal Engineering*, *40*(3), 161–182. doi:https://doi.org/10.1016/s0378-3839(00)00007-7

De Ridder, M.P., J. Kramer, J.P. den Bieman & I. Wenneker, 2022. Validation and practical application of nonlinear wave decomposition methods for irregular waves. (under review)

Deltares, 2022a. Wave run-up velocities – derivation of an expression to be used in the cumulative overload method. Deltares report 11208057-037-GEO-0002. Authors: J.P. den Bieman and M.W. Doeleman. (draft)

Deltares, 2022b. Consequentieanalyse van een nieuwe uitdrukking voor stroomsnelheden in de cumulatieve overbelastingmethode – voor de initiële mechanismen GEKB en GEBU oploopzone (in Dutch). Deltares report 11208057-037-GEO-0005. Authors: A.J. Smale and J.P. den Bieman. (draft)

Deltares, 2022c. Parameters flow velocities on dike slopes – Analysis of influence factors on wave run-up and overtopping flow velocities. Deltares report 112034-001-ZWS-0003. Authors: N. Huppes and V.M. van Bergeijk. (draft)

Deltares, 2019. Invloed waterdiepte op golfoverslag: numerieke studie. M. de Ridder and P. van Steeg. Deltares rapport 11203682-015-ZWK-0001, 29 oktober 2019, definitief.

Deltares, 2018. Invloed waterdiepte op golfoverslag: meetverslag golfoverslag proeven. M. de Ridder and P. van Steeg. Deltares rapport 11202189-012-ZWS-0001, 7 December 2018, definitief.

Den Bieman, J.P, M.P. de Ridder & M.R.A. van Gent, 2020. Deep learning video analysis as measurement technique in physical models. Coastal Engineering 158, 103689. doi: https://doi.org/10.1016/j.coastaleng.2020.103689

Eldrup, M. R., & Lykke Andersen, T., 2018. Estimation of Incident and Reflected Wave Trains in Highly Nonlinear Two-Dimensional Irregular Waves. Journal of Waterway, Port, Coastal, and Ocean Engineering, 145, 04018038. doi:https://doi.org/10.1061/(ASCE)WW.1943-5460.0000497

EurOtop, 2018. Manual on wave overtopping of sea defences and related structures, Van der Meer, J.W., Allsop, N.W.H., Bruce, T., De Rouck, J., Kortenhaus, A., Pullen, T., Schüttrumpf, H., Troch, P., Zanuttigh, B. (Eds), www.overtopping-manual.

Gent, Marcel & Caires, Sofia., 2011. Individual Wave Height Distribution in Constant and Finite Depth Regions. Proceedings of the International Offshore and Polar Engineering Conference.

Holthuijsen, L. H., 2007. *Waves in oceanic and coastal waters*. Cambridge: Cambridge University Press.

Jacobsen, N.G., Fuhrman, D.R., Fredsøe, J., 2012. A wave generation toolbox for the open-source CFD library: openFoam®. Int. J. Numer. Methods Fluids 70, 1073–1088.

Karmpadakis, I., Swan, C., & Christou, M., 2022. A new wave height distribution for intermediate and shallow water depths. *Coastal Engineering*, *175*, 104130. https://doi.org/10.1016/j.coastaleng.2022.104130

Lashley, C. H., 2021. The Influence of Infragravity Waves on Overtopping at Coastal Structures with Shallow Foreshores. https://doi.org/10.4233/uuid:f93143bc-0214-41ad-af4a-4ad2168a42a5

Lashley, C. H., Jonkman, S. N., van der Meer, J., Bricker, J. D., and Vuik, V., 2022. The influence of infragravity waves on the safety of coastal defences: a case study of the Dutch Wadden Sea, Nat. Hazards Earth Syst. Sci., 22, 1–22, https://doi.org/10.5194/nhess-22-1-2022.

Longuet-Higgins, M. S., 1952. On the statistical distribution of the heights of sea waves. Journal of Marine Research, 11, 245–266.

TAW, 2002. Technical Report Wave Run-Up and Wave Overtopping At Dikes. Technical Advisory Committee on Flood Defences, Delft, The Netherlands.

Van Gent, M.R.A., 1999. "Physical model investigations on coastal structures with shallow foreshores: 2D model tests with single and double-peaked wave energy spectra." *Hydraulic Engineering Reports*,Delft

Van Steeg, P., de Ridder, M., Capel, A. en M. Bottema., 2020. Influence of water depth on wave overtopping. Proceeding FLOODrisk 2020. DOI 10.3311/FloodRisk2020.1.25

A Additional information datasets

In this appendix the model set-up of the three datasets is shown. Also, some additional information, such as the test program, of the Delta Flume 2022 experiments is given.

A.1 Scheldt Flume 2018

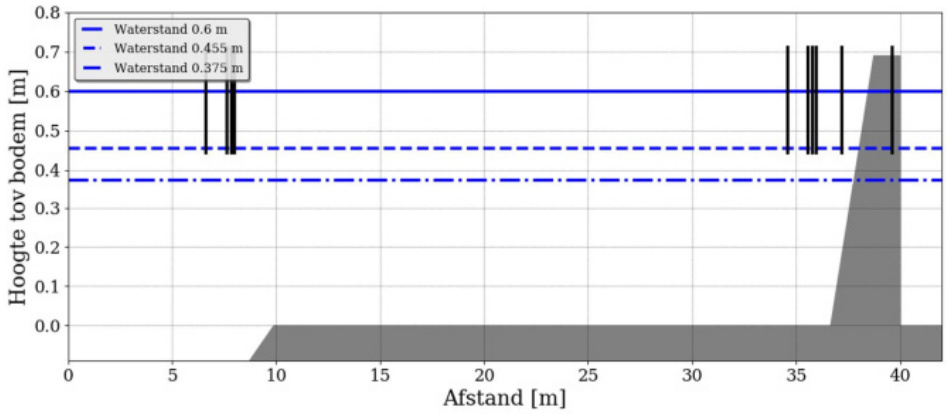

Figure A.1 Model set-up of the physical experiments in the Scheldt Flume (Deltares, 2018)

A.2 Scheldt Flume OpenFOAM 2019

Figure A.2 Model set-up of the numerical simulations based on the Scheldt Flume 2018 experiments (Deltares, 2019). The model is composed of an OceanWave3D domain (left) and OpenFOAM domain (right) to reduce the computation time.

A.3 Delta Flume 2022

The model set-up of the Delta Flume 2022 experiments is shown in Figure A.3. The vertical lines at 120 meter horizontal distance represent a set of wave gauges. It is noted that in this research, run-up events above 7.6 meters on the dike are considered as overtopping events to eliminate possible effects of different dike slopes.

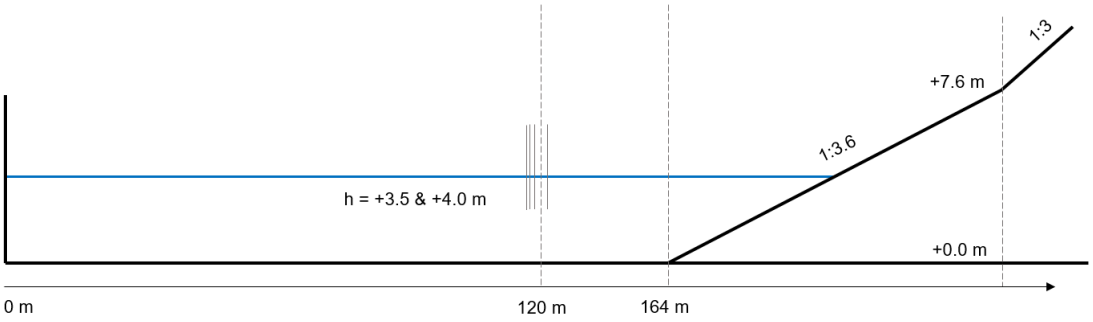

Figure A.3 Model set-up of the Delta Flume 2022 experiments.

Table A.1: Test program of the Delta Flume 2022 experiments with measured parameters.

	Water depth	H_{m0}	T_p	$T_{m-1,0}$	$S_{m-1,0}$	H_{m0}/d	$\xi_{m-1,0}$
T102	4.0	0.4	3.4	3.3	0.024	0.1	1.79
T103	3.5	0.32	2.4	2.2	0.043	0.1	1.34
T111	3.5	0.94	8.3	7.6	0.01	0.27	2.72
T112	3.5	0.89	5.3	5.2	0.021	0.25	1.90
T121a	3.5	1.2	9.1	8.3	0.011	0.34	2.64
T122	3.5	1.17	6.3	6.2	0.02	0.34	1.97
T123	3.5	1.11	4.3	4.2	0.04	0.32	1.38

B Data handling

In this appendix the methods of data analysis are described. First the data handling of all different measurement techniques is described. Secondly, the detection of discrete wave run-up events is elaborated upon. Lastly, the derivation of the front velocities is shown. This appendix corresponds with chapter 4 of Deltares (2022a).

B.1 Data handling per measurement technique

In Chapter 2, all available datasets that include the possibility to derive wave run-up signals have been listed. The measurement techniques include video measurements (dataset 1 and 3) and numerical data (dataset 2).

B.1.1 Video measurements

In datasets 1 and 3, described in Chapter 3, the wave run-up is measured using video cameras combined with the deep learning video analysis technique described by Den Bieman *et al.* (2020). This technique uses computer vision methods to teach an automated segmentation algorithm to detect the position wave run-up front in the captured video imagery. In this way, a time series of the front position can be generated for the entire video. From this wave run-up time signal, the front velocity can be derived, as is described in Section 4.3.

To train the deep learning method, the algorithm is fed examples of successfully segmented images of the wave run-up front. This data set is split, where 80\% is used for the actual training of the deep learning model, and the remaining 20\% is used to determine when the training should be stopped to prevent overfitting. The application of the deep learning method to wave run-up has been validated in Den Bieman *et al.* (2020), where the results for the wave run-up height from the method were compared to visual observations.

B.1.2 Numerical data

One dataset is simulated using the numerical OpenFOAM toolbox. To derive the runup and velocities, the model output from numerical wave gauges (dataset 2) and water fraction probes is used. The steps to process the OpenFOAM output per simulation to a run-up signal is listed below

1. Create continuous array of the output (in case of multiple files per simulation)
2. Define vertical positions of the output locations along the slope using the x-coordinates of the output and the structure coordinates. This is shown in Figure B.1.
3. Interpolate the output to an equally spaced time signal with a reduced timestep of 200 Hz
4. Per timestep, identify the maximum height (y-coordinate) that exceeds the threshold water layer thickness (0.5 millimetre for wave gauges and 60% water fraction for the probes). This is illustrated in Figure B.1. At t = 50 seconds, the water layer thickness or water fraction is larger than its threshold. The run-up level is therefore y = 0.2 meter.
5. Clean the obtained step gauge signal following section B.1.3.
6. Average the 200 Hz clean step gauge signal using the moving mean function over 10 timesteps (probes) or 20 timesteps (wave gauges) to remove unphysical wiggles and spikes.

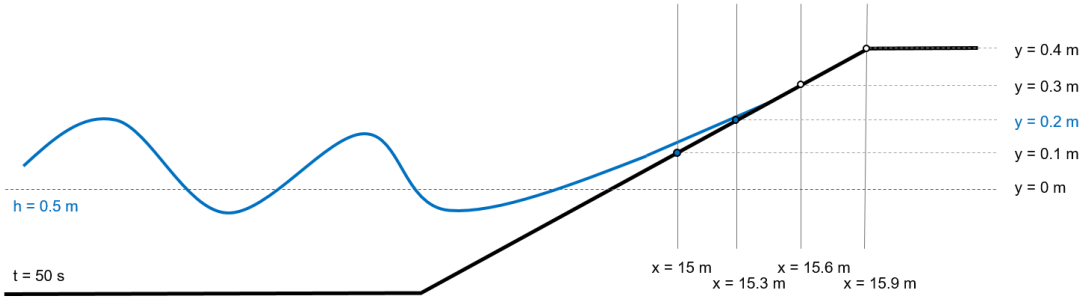

Figure B.1 Schematic visualisation of the numerical output processing technique

B.1.3 Step gauge processing

The output signal of the step gauge takes the shape of a staircase as the run-up height is only given at the locations of the pins and not continuously in space. To obtain a smooth and physical realistic signal, the first point in time of the ascending staircase are taken and the last point of descending staircase. At the top of the staircase, no points are removed and a horizontal plateau remains. This is illustrated in Figure B.2.

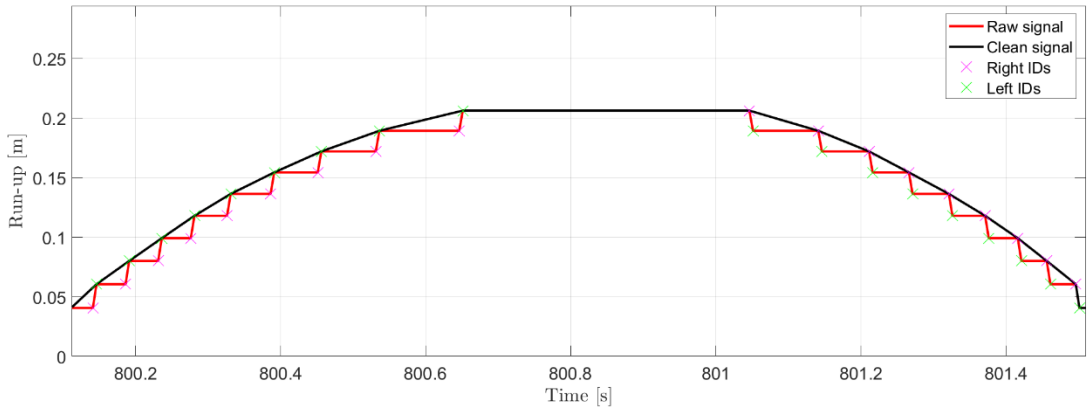

Figure B.2 Processing the step gauge signal (red) to a smooth and physically realistic wave run-up signal (black)

It is noted that in the detection of the maximum run-up height, discussed in section B.2, the maximum run-up height per run-up event is corrected by adding half the distance of the respective output location and the next output location. The reasoning is that the run-up height is at minimum the height of the last wet output location and at maximum the height of the first dry output location, there is an underestimation of the maximum run-up level without this correction. As the distance between the output locations are small, the difference between the results with and without correction is small. Note that run-up events that give a signal on the last (highest) output location are considered to result in wave overtopping.

B.2 Wave run-up event detection

The starting point for the detection of individual wave run-up events is the wave run-up time signal processed (depending on measurement instrument) as described in Section 4.1. This time signal is then lightly smoothed by taking the 3-point simple moving average (SMA) of the signal. On this signal, a peak-over-threshold method with a time-varying threshold is applied. A time-varying threshold is necessary due to the water level variations caused by wave groups and bound long waves. If a constant threshold would be used, a lot of run-up events would be missed because either the maximum run-up height is below the threshold, or the minimum run-down level is above is. The time-varying threshold used is a SMA with a moving window of 2 spectral wave periods ($T_{m-1,0}$), an example of which is shown in Figure B.3.

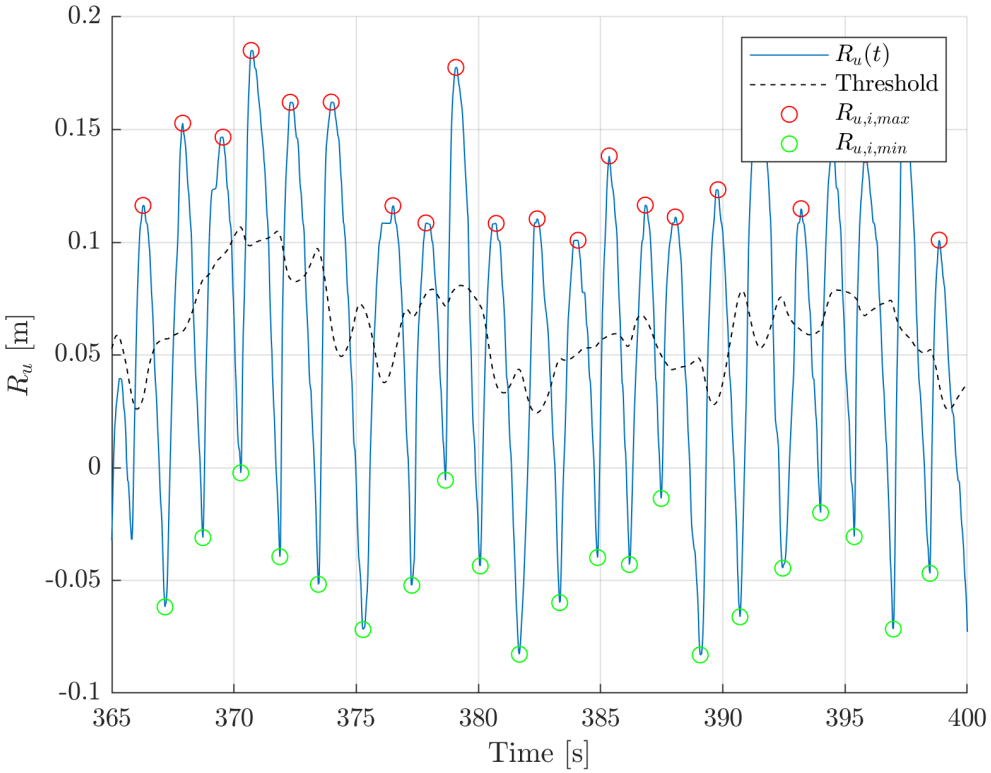

Figure B.3 Example of the detection of individual wave run-up events.

For each peak that exceeds the time-varying threshold the maximum value is determined (the red circles in Figure B.3), resulting in the maximum wave run-up height per wave run-up event. Next, the minimum run-up height is determined in between two subsequent peaks (the green circles in Figure B.3). Now a wave run-up event is defined as starting at a green circle and ending at a red circle. This means the wave run-down (from red to green circle) is disregarded in the rest of this report, as the wave run-down is out of scope.

B.2.1 Dealing with overtopping events

In some of the data sets listed in Chapter 3, some of the waves running up the outer slope will also overtop the dike crest. An event is considered to overtop when either a) the run-up height exceeds the crest level ($R_u > R_c$) or b) when the run-up height is equal to the maximum run-up height in the range of the measurement instrument used.

For these overtopping events, the maximum wave run-up height cannot be determined. Hence, for the purposes of wave run-up height exceedance these events are counted as NaN (not-a-number) values for which $R_u > R_c$ (the missing events are located on the high run-up side of the exceedance curve). These overtopping events are also disregarded in determining the development of the velocity per event over the outer slope.

When determining the maximum wave run-up front velocity, the run-up events that lead to wave overtopping are still used. The reasoning behind this is that the maximum front velocity for an event does not occur at or close to the maximum run-up height for that event, and the data sets considered do not feature very low relative crest heights. Hence, the maximum front velocity should still be captured during overtopping events, even though the maximum run-up height is not.

B.3 Derivation of the wave run-up front velocity

For each wave run-up event (as defined in Section B.2) the front velocity is calculated using (first order) central differencing, which uses the run-up height of the previous and subsequent time step to calculate the velocity. In this way, there is a small amount of additional smoothing of the signal, but the link between the velocity and the location on the slope it occurs is conserved as much as possible.

As mentioned above, the front velocity is derived from the run-up height signal (accounting for the dike slope). Hence, relatively small errors and inaccuracies in the run-up signal can translate into large ones in the front velocity signal (because the velocity is based on the derivative). To filter out potential unrealistically high velocities, a maximum acceleration factor is introduced. The reasoning behind this is that the acceleration (and deceleration) of the wave run-up front is capped and should realistically remain within X times the median acceleration present in the signal. The acceleration of the time signal is derived in a similar way as the velocity itself, by central differencing. The parts of the velocity signal for which the acceleration is higher than permitted by the maximum acceleration factor – including the time step before and after (because they are used in the central differencing in the velocity signal) – are disregarded in the further analysis. The allowable maximum acceleration factor can differ a bit based on the wave conditions and measurement instrument, so they are determined per test.

C Additional figures for relationship assessment

In this appendix the relation between the wave height and wave *run-up* height distribution is shows for all tests.

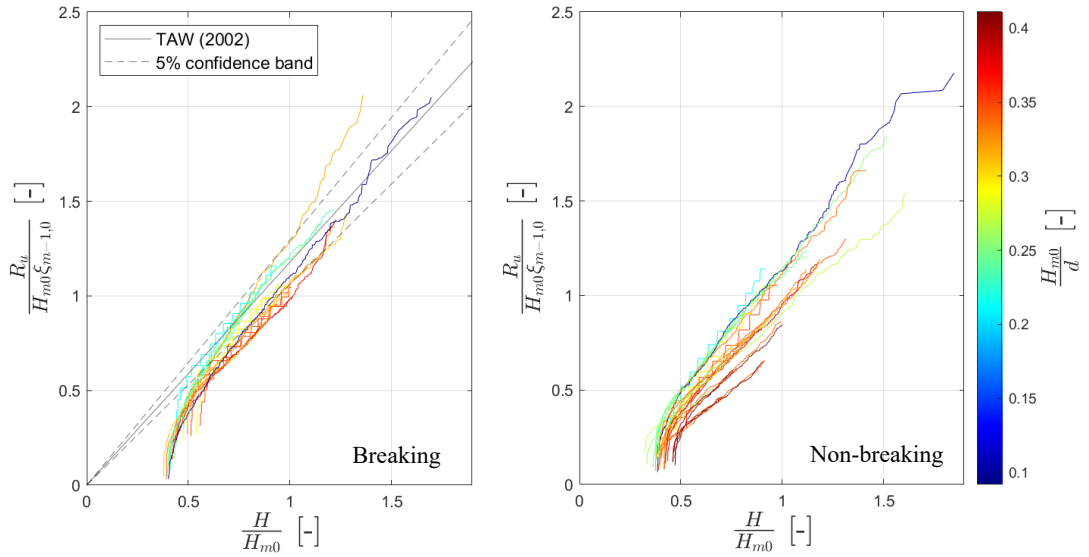

Table C.1 The normalised measured wave run-up height (y-axis) versus the normalised measured wave height (x-axis) exceedance distribution for the selected tests with breaking waves (left panel) and non-breaking waves (right panel). The relative water depth is shown in colour with blue a relatively deep, and red a relatively shallow foreshore. In the left panel the TAW (2002) prediction including the 5% confidence band is shown.

D Wave run-up and velocities per dataset

Assessing the influence of the relative water depth on the wave run-up and front velocities per dataset. In order to eliminate additional dataset related factors. This supports the conclusion that no trend in relative water depth can be observed. In this appendix no distinction is made between breaking and non-breaking waves (TAW, 2002).

D.1 Wave run-up height versus front velocity distribution

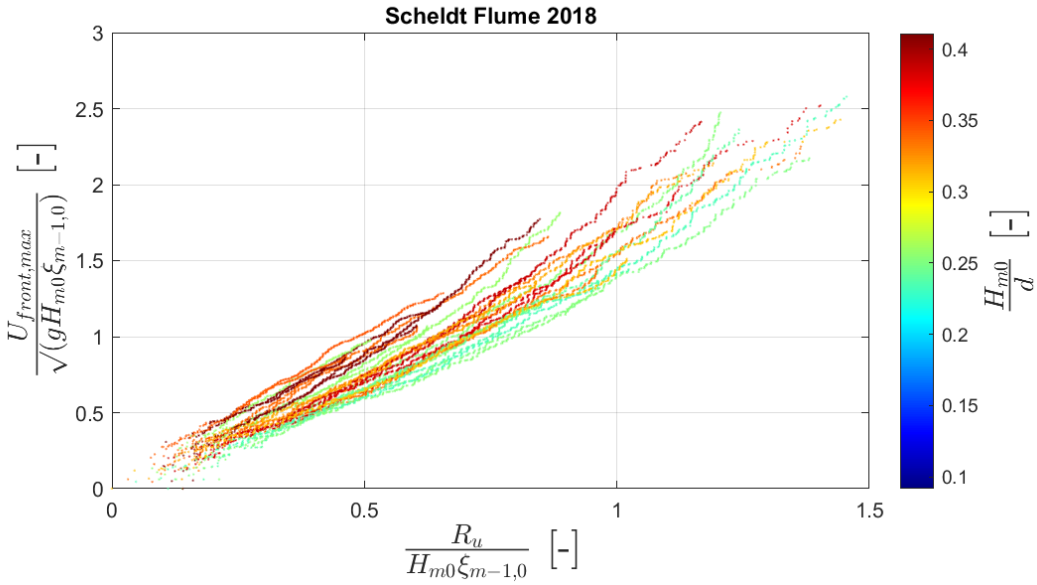

Figure D.1 The normalised front velocity (y-axis) versus the normalised wave run-up height (x-axis) exceedance distribution for the physical Scheldt Flume 2018 tests. The relative water depth is shown in colour with blue a relatively deep, and red a relatively shallow foreshore.

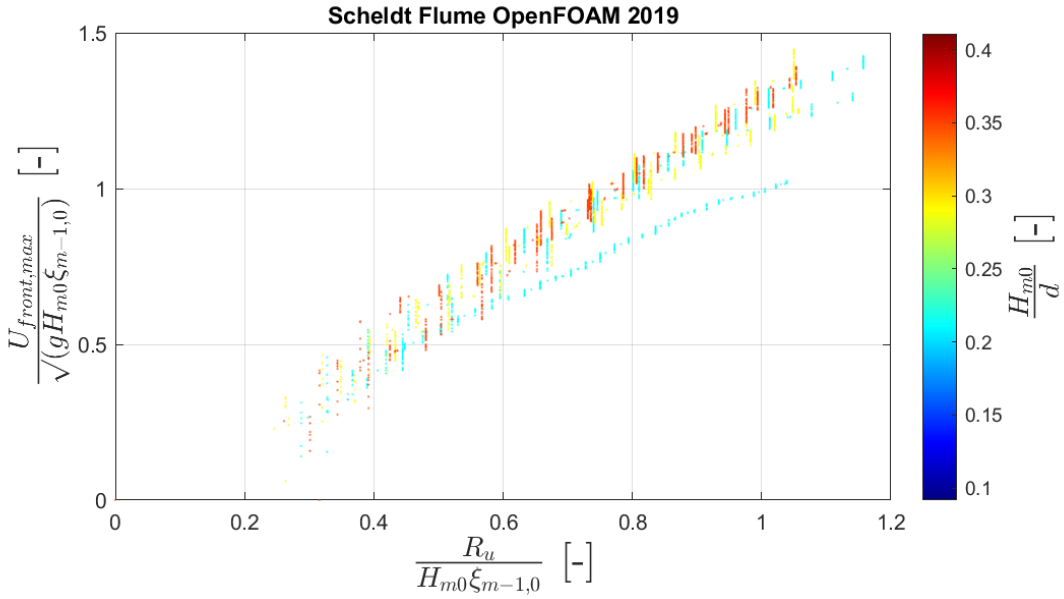

Figure D.2 The normalised front velocity (y-axis) versus the normalised wave run-up height (x-axis) exceedance distribution for the numerical Scheldt Flume 2019 tests. The relative water depth is shown in colour with blue a relatively deep, and red a relatively shallow foreshore.

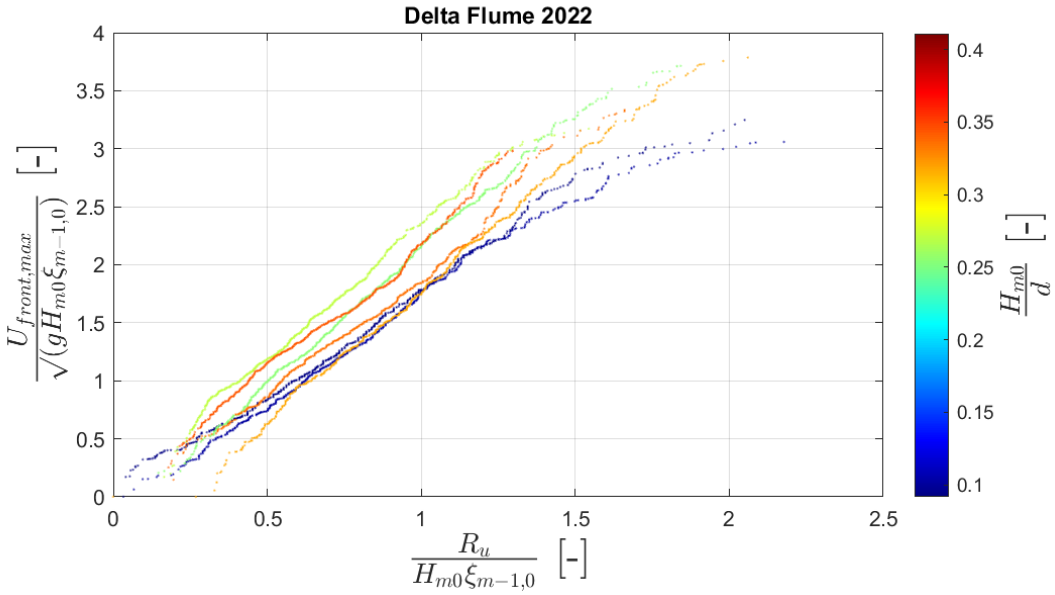

Figure D.3 The normalised front velocity (y-axis) versus the normalised wave run-up height (x-axis) exceedance distribution for all Delta Flume 2022 tests. The relative water depth is shown in colour with blue a relatively deep, and red a relatively shallow foreshore.

D.2 Event based wave run-up height versus front velocities

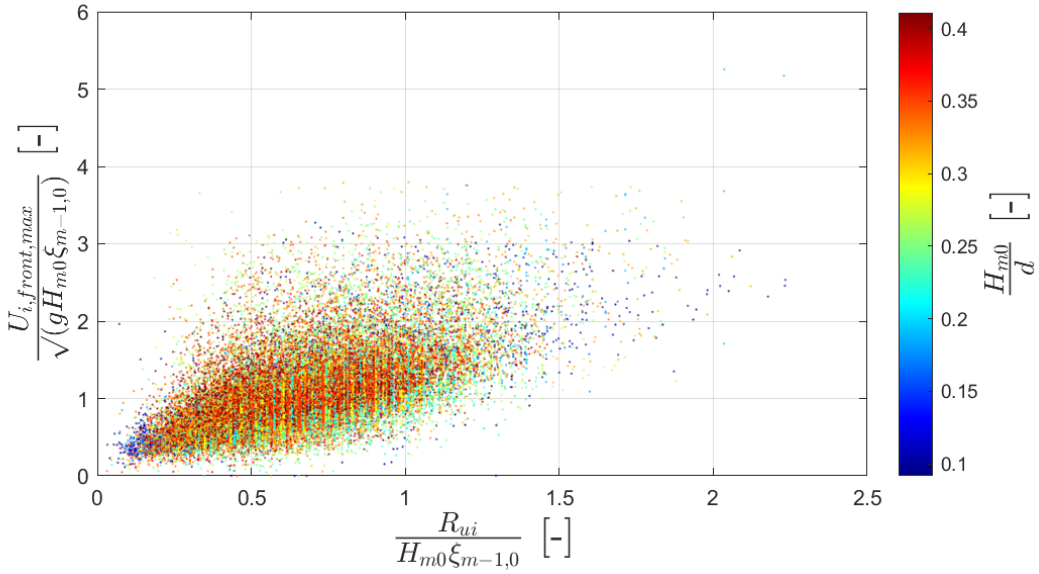

Figure D.4 The normalised front velocity events (y-axis) versus the normalised wave run-up height events (x-axis) for all tests. The relative water depth is shown in colour with blue a relatively deep, and red a relatively shallow foreshore.

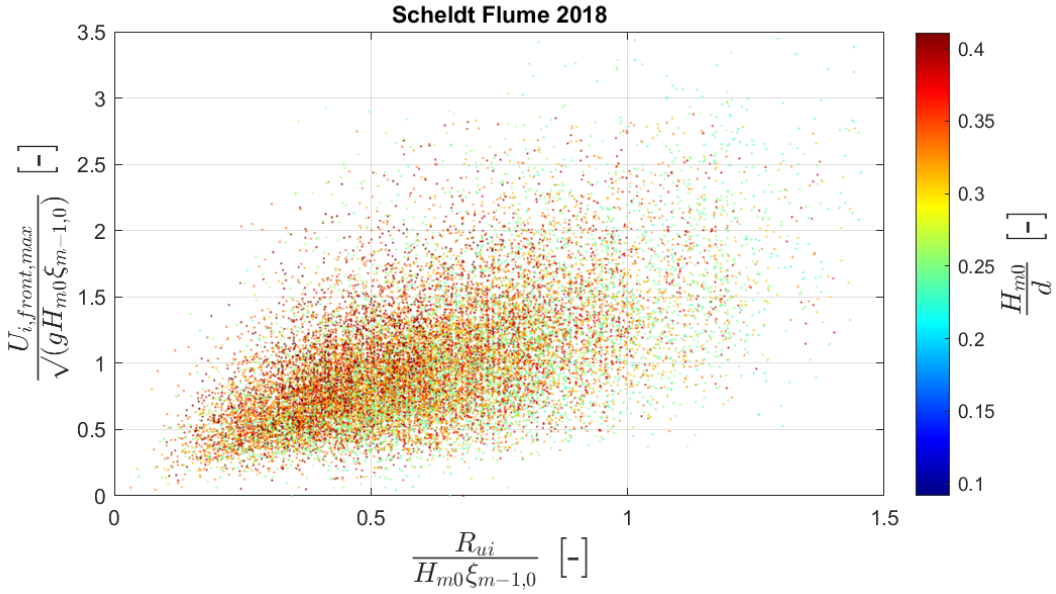

Figure D.5 The normalised front velocity events (y-axis) versus the normalised wave run-up height events (x-axis) for all physical Scheldt Flume 2018 tests. The relative water depth is shown in colour with blue a relatively deep, and red a relatively shallow foreshore.

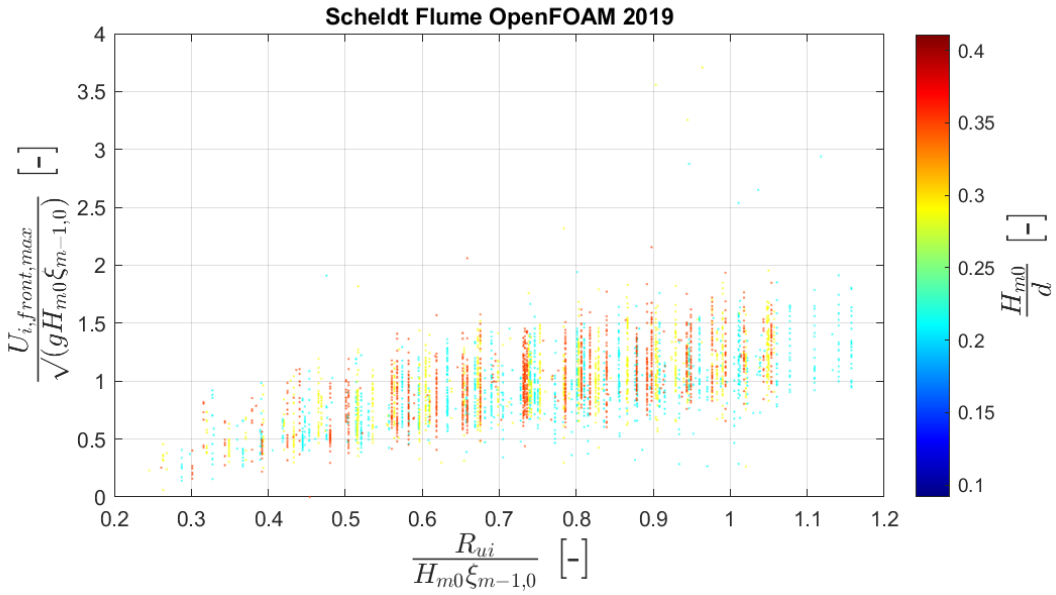

Figure D.6 The normalised front velocity events (y-axis) versus the normalised wave run-up height events (x-axis) for all numerical Scheldt Flume 2019 tests. The relative water depth is shown in colour with blue a relatively deep, and red a relatively shallow foreshore.

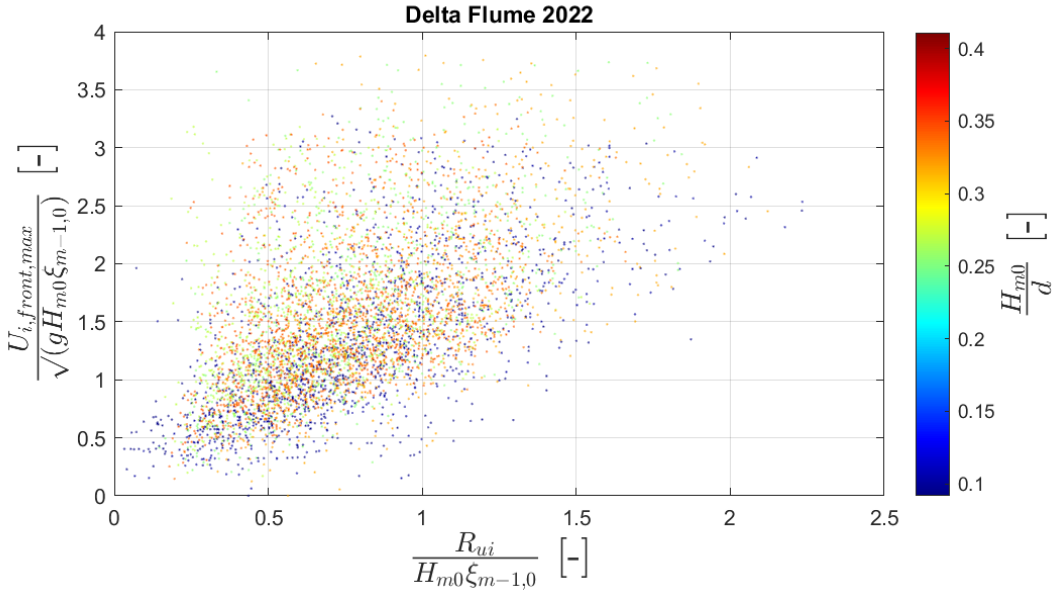

Figure D.7 The normalised front velocity events (y-axis) versus the normalised wave run-up height events (x-axis) for all Delta Flume 2022 tests. The relative water depth is shown in colour with blue a relatively deep, and red a relatively shallow foreshore.

Deltares is an independent institute for applied research in the field of water and subsurface. Throughout the world, we work on smart solutions for people, environment and society.

Deltares

www.deltares.nl